NUMERICAL SIMULATION OF HIGH STRENGTH COLD-FORMED SUPACEE® SECTIONS IN COMBINED BENDING AND SHEAR

CAO HUNG PHAM & GREGORY J. HANCOCK

SCHOOL OF CIVIL ENGINEERING

THE UNIVERSITY OF SYDNEY

THE UNIVERSITY OF SYDNEY

NUMERICAL SIMULATION OF HIGH STRENGTH COLD-FORMED SUPACEE® SECTIONS IN COMBINED BENDING AND SHEAR

RESEARCH REPORT R913

CAO HUNG PHAM
GREGORY J. HANCOCK

February 2010

Copyright Notice

ABSTRACT

The report describes numerical non-linear simulation, based on the finite element method (FEM) using the software package ABAQUS/Standard, of high strength cold-formed SupaCee sections in shear, combined bending and shear, and bending only. These high strength (450 MPa) C-profile steel sections called SupaCee® contain additional return lips and web stiffeners which enhance the bending and shear capacity of the sections (Lysaght, 2003). They are used widely in Australia as purlins in roof and wall systems.

The results of nonlinear analyses by using the finite element method (FEM) depend heavily on the imperfection assumption for the analysis of the thin-walled members. Geometric imperfections are often taken as a scaled multiple of the eigenvalue modes. Different buckling modes (Mode 1 Anti-Symmetric and Mode 2 Symmetric) are assumed with different magnitude levels of imperfection as proposed by Camotim in Portugal and Schafer in the USA. Studies of the effects of boundary condition, element types as well as mesh size are also included.

This report summarises the results of the finite element nonlinear simulations of the tests on SupaCee® sections performed at the University of Sydney on a variety of section sizes and thicknesses. The test series include predominantly shear *(V)*, combined bending and shear *(MV)*, and bending only *(M)* test series. The FEM results are compared with the tests to calibrate the imperfection magnitudes and modes against the tests. Conclusions regarding the size and type of imperfection are made in the report. It is demonstrated that the finite element analysis can therefore be used to design and optimize thin-walled sections of high strength steel.

KEYWORDS

TABLE OF CONTENTS

INTRODUCTION

Numerical simulation using the Finite Element Method (FEM) of thin-walled cold-formed steel sections undergoing buckling depends substantially on assumptions regarding boundary conditions, initial geometric imperfections, element mesh and type. For high strength sections in compression (Yang and Hancock, 2006), accurate simulations have been achieved by using ABAQUS (HKS 1997). For sections in bending, Yu (2005) provided complete details of the finite element models consisting of shell elements to investigate the influence of the test setup on the buckling modes of cold-formed steel members in bending and additional nonlinear analysis is also included.

For sections in shear, and combined bending and shear, an accurate simulation (Pham and Hancock, 2010a) has been recently reported to calibrate against tests of an experimental investigation on normal plain lipped C-section steel purlins performed at the University of Sydney (Pham and Hancock, 2009). The main objectives of this testing program are to summarise proposals for extension of the Direct Strength Method (DSM) (Schafer and Peköz, 1998) to shear and combined bending and shear. The DSM was formally adopted in the North American Design Specification in 2004 and in AS/NZS 4600:2005 as an alternative to the traditional Effective Width Method (EWM) in 2005. It uses elastic buckling solutions for the entire member cross section to give the direct strength rather than for elements in isolation.

As sections become more complex with additional multiple longitudinal web stiffeners and return lips as included in SupaCee® sections, the computation of the effective widths becomes more complex. For the EWM, the calculation of effective widths of the numerous sub-elements leads to severe complications with decreased accuracy. In some special cases, no design approach is even available for such a section using the EWM. The DSM appears to be more beneficial and simpler by using the elastic buckling stresses of the whole complex channel sections such as the SupaCee® section.

In order to further understand the DSM in shear, another experimental program (Pham and Hancock, 2010b) has been recently performed at the University of Sydney for SupaCee® sections. The test series included predominantly shear (*V*-series), combined bending and shear (*MV*-series), and bending only (*M*-series). Two different commercially available depths (150, 200 mm) and three different thicknesses (1.2, 1.5, 2.4 mm) of SupaCee® channel sections. Tests with and without torsion/distortion restraint straps screwed on the top flanges adjacent to the loading points were also considered.

This report presents the modeling and analysis of the experimental SupaCee® specimens of *V*, *MV*, and *M* test series by using the Finite Element Method (FEM) program ABAQUS. The effects of such input parameters as initial geometric imperfection, element type and the size of element mesh on the convergence of the solution have been investigated. Experimental data from (Pham and Hancock, 2010b) was utilized to evaluate the performance of the FE model. The accurate results of the numerical simulation show that the finite element analysis can be utilized to predict the ultimate loads which include the post-buckling behavior of cold-formed purlins in shear and under combined bending and shear.

FINITE-ELEMENT SIMULATION

GENERAL

A detailed FE model has been developed to study the structural behavior of high strength cold-formed SupaCee® purlins in shear, and combined bending and shear, and bending only. In order to obtain realistic models, for the finite element non-linear analysis, plastic strains are included. Tensile coupons were tested to determine the stress-strain curves and the plastic strain data of the sections tested by Pham and Hancock (2010b).

The commercially available software package ABAQUS/Standard (2008) version 6.8-2 was used to develop the FE models. The simulation consists of two steps. In the first step, an elastic buckling analysis, called a Linear Perturbation analysis, was performed on a perfect purlin to obtain its buckling modes (eigenmodes). This shows the possible buckling modes of the structure. The second step was a non-linear analysis using the modified Riks method. Material plasticity strains and geometric imperfection based on the eigenmodes are included in the analysis to obtain the ultimate failure loads and failure modes of purlins in shear, under combined bending and shear, and bending only. Although, the channel section members were symmetrically

tested in pairs with flanges facing inwards and with a gap between them to ensure inside assembly was possible, only one channel beam was modelled in order to save computational time.

MATERIAL PROPERTIES AND MATERIAL ORIENTATION

In the non-linear analysis, ABAQUS requires the input of the material stress-strain curves in the form of true stress σ_{true} versus true plastic strain ε_t. The true stress (σ_{true}) and true plastic strain (ε_{true}) were converted from the engineering stresses (σ) and engineering strains (ε) as follows:

$$\sigma_{true} = \sigma(1+\varepsilon) \tag{1}$$

$$\varepsilon_{true} = \ln(1+\varepsilon) - \frac{\sigma_{true}}{E} \tag{2}$$

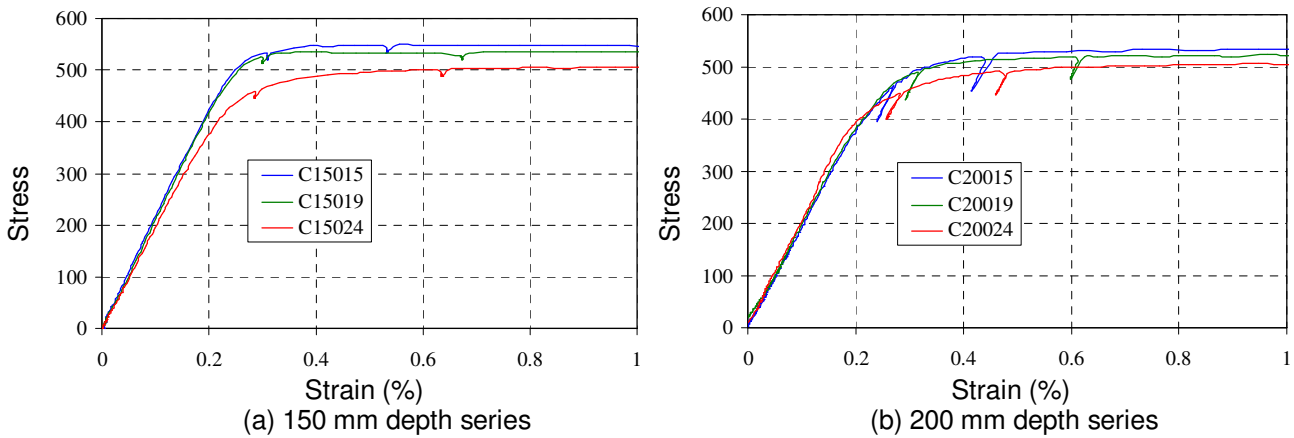(a) 150 mm depth series   (b) 200 mm depth series

Figure 1. Longitudinal tension (engineering) stress-strain curves

where E is the Young's modulus, σ and ε are engineering stress and strain respectively (ABAQUS, 2008). The measured stress and strain curves were based on tensile coupon tests conducted by Pham and Hancock (2010b) and are shown in Fig. 1 for each of the section sizes tested. The yield stress f_y was obtained by using the 0.2 % nominal proof stress.

In order to determine the longitudinal stress distributions in the postbuckling range, the material has to be oriented into the longitudinal direction. This is implemented by assigning the material with a local coordinate system by using the *ORIENTATION option in ABAQUS. During the orientation, each element is assigned to have the member 2-axis of the coordinate system in the longitudinal direction.

TEST RIG CONFIGURATION AND SPECIMEN BOUNDARY CONDITIONS

The basic design of the test rig was that developed by LaBoube and Yu (1978). A diagram of the test set-up is shown in Fig 2 for both the *V* and *MV* series. The only difference between the *V* and *MV* tests is the ratio of shear span to depth where the shear span is the distance between the lines of bolts at the loading and support points. With the *V* series, the ratio of span to depth is 1:1 whereas that of *MV* series is 2:1. For the *M* series, the four point bending arrangement provided a central region of uniform bending moment and zero shear force as shown in Fig. 3. Tests with and without straps screwed adjacent to the loading points are shown in Fig. 4. All tests were performed in the 2000 kN capacity DARTEC testing machine, using a servo-controlled hydraulic ram.

The channel section members were tested in pairs with flanges facing inwards and with a gap between them to ensure inside assembly was possible. At the supports, the test two beam specimens were bolted through the webs by vertical rows of M12 high tensile bolts. These rows of bolts were connected to two channel sections 250x90x6CC with stiffeners. Steel plates of 20 mm thickness were used as load transfer plates which were also bolted through the flanges of the channel sections 250x90x6CC with stiffeners. These load bearing plates rested on the half rounds of the DARTEC supports to simulate a set of simple supports as shown in Fig. 5(a).

This test rig is modelled explicitly by using 3D deformable solid members which were made using normal steel properties. All M12 high tensile bolts of 830 MPa for Grade 8.8 were pretensioned up to 90 kNm torque to prevent slip under initial loading. In order to model these contacts, the "tie" constraints were used to model contacts between the specimens and rigs where the the channels were the slave surfaces and the rigs were the master surfaces. The simply supported boundary conditions of the loading bearing plates resting on the half rounds of DARTEC supports were simulated in the ABAQUS model as shown in Fig. 5(b). "CONN3D2" connector elements were used to connect the bearing plates to the centre of the half round. Both ends of connector elements are hinges and the length of the shortest connector member is the radius of half round.
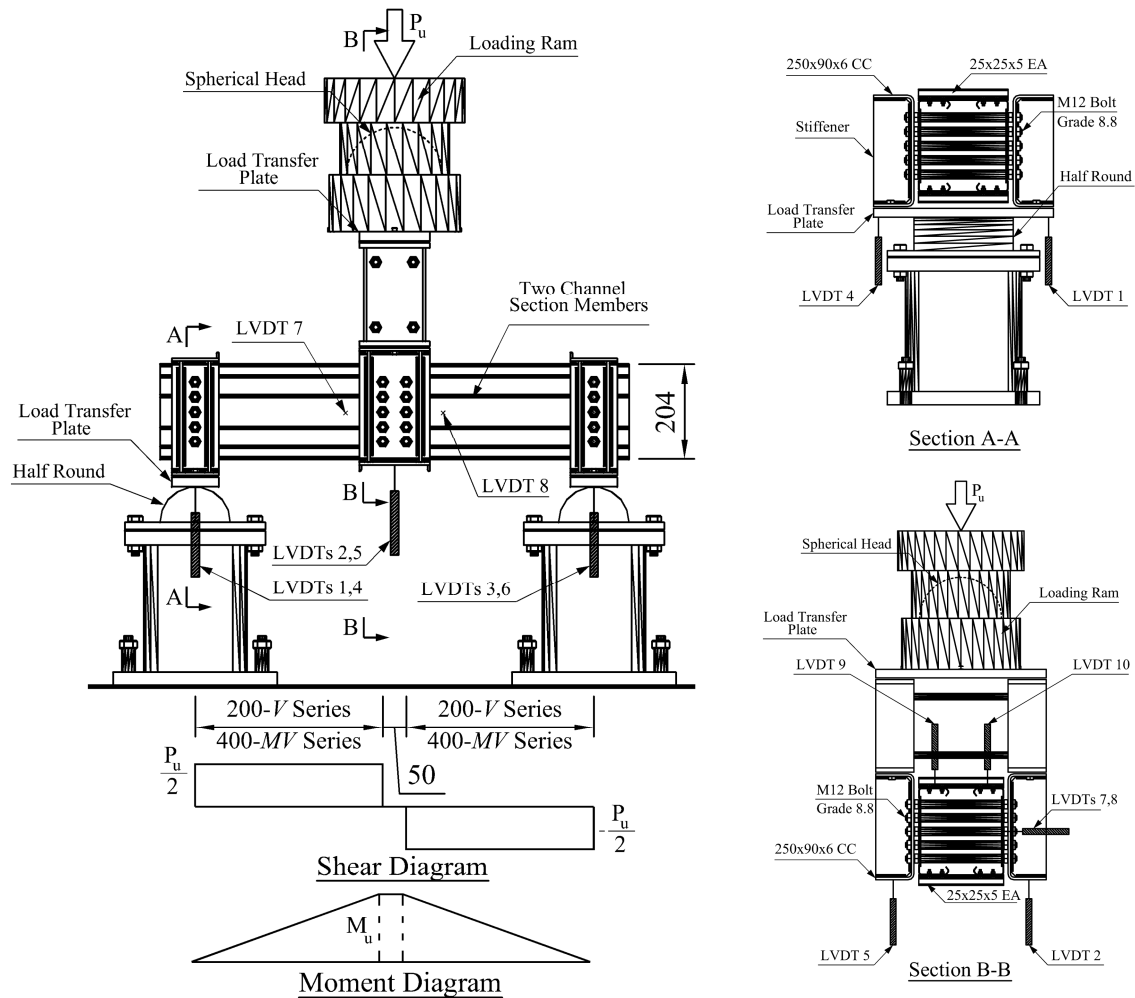
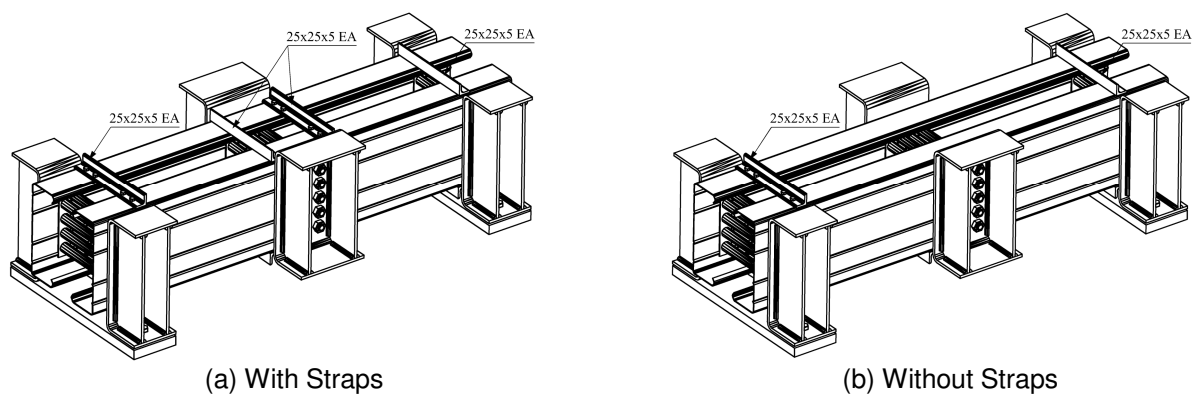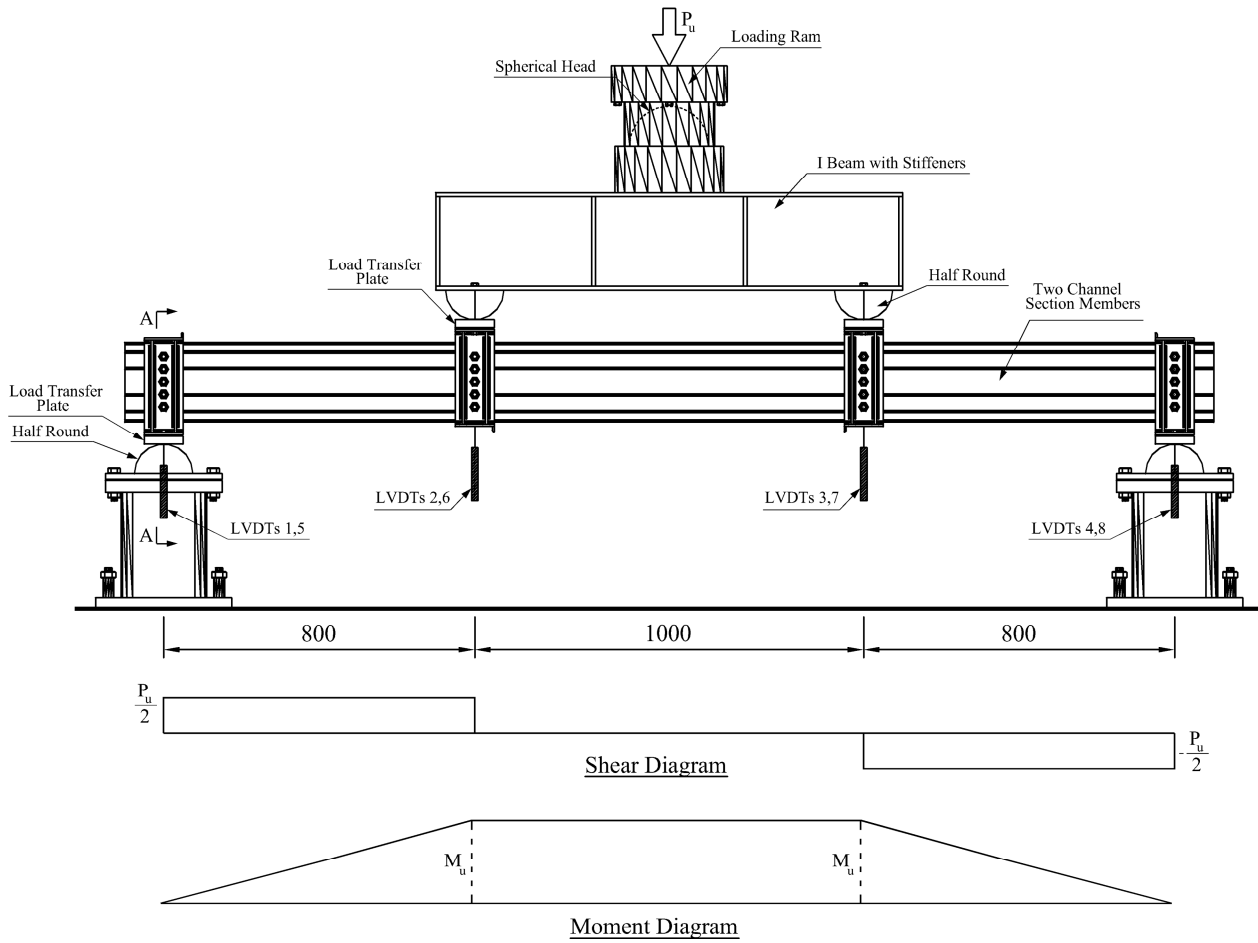Figure 2. *V* and *MV* Test Series Configuration (200 mm Deep Sections)

Figure 3. *M* Test Series Configuration (200 mm Deep Sections)

(a) With Straps

(b) Without Straps

Figure 4. Tests with and without Straps Configuration

(a) Test Support

Half round center
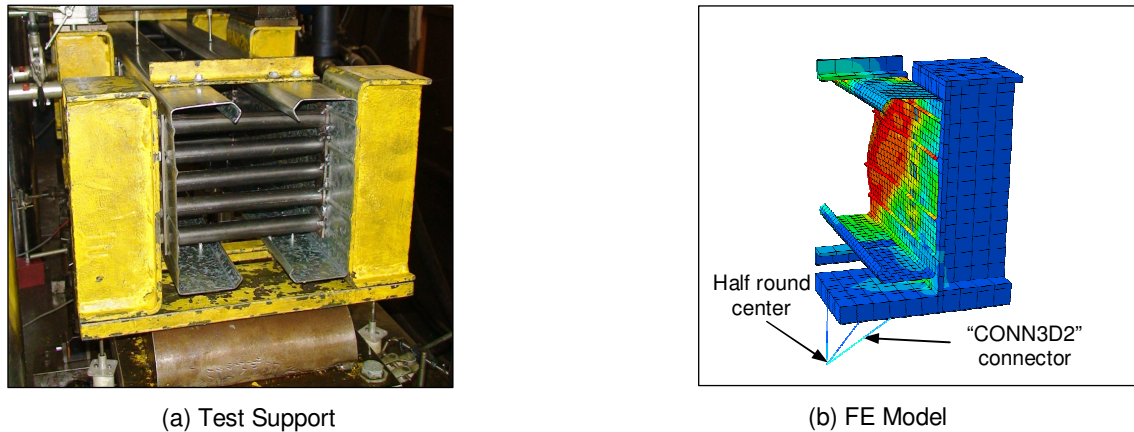
"CONN3D2" connector

(b) FE Model

Figure 5. Specimen and ABAQUS Boundary Conditions

At the loading point at mid-span, the DARTEC loading ram has a spherical head to ensure that the load is applied uniformly on the bearing plate. The load was transferred to two channel sections 250x90x6CC with stiffeners which were connected to the test beam specimens by two vertical rows of M12 high tensile bolts. In the ABAQUS model, loads were directly applied at the bolt positions to simulate the load transferring from the loading ram to the channel section via the 250x90x6CC channel sections.

INITIAL GEOMETRICAL IMPERFECTION

In the non-linear analysis, imperfections are usually introduced by perturbations in the geometry. Initial geometrical imperfections are added onto the "perfect" model to create out-of-plane deformations of the plate elements. In the ABAQUS model, there are three methods to define the geometric imperfecitons. Firstly, the geometric imperfections can be defined by the linear superposition of buckling eigenmodes. Secondly, specifying the node number and imperfection values directly on the data lines gives a method of direct entry. The final method is defined by the displacements from an initial *STATIC analysis, which may consist of the application of a "dead" load.

In this report, the first method employing the linear superposition of buckling modes is used. An initial analysis is carried out on a perfect mesh using the elastic buckling analysis to generate the possible buckling modes and nodal displacements of these modes. The imperfections are introduced to the perfect mesh by means of linearly superimposing the elastic buckling modes onto the mesh. The lowest buckling modes are usually the critical modes and these are, therefore, used to generate the imperfections. The coordinates of the eigenmodes obtained from this analysis are by default stored in a file with extension *.fil and can subsequently be used as input for the *IMPERFECTION command in the actual simulation with different scaling factors with respect to the thickness of the channel. The imperfection magnitudes were based on two scaling factors of 0.15t and 0.64t with both positive and negative signs where t is the thickness of channel section. These two factors were proposed by Silvestre and Camotim (2004) and Schafer and Pekoz (1998) respectively.

EIGENVALUE BUCKLING ANALYSIS PREDICTION AND POST-BUCKLING ANALYSIS

Eigenvalue buckling analysis is generally used to estimate the critical buckling loads of a stiff structure. ABAQUS uses the subspace iteration eigensolver when the *BUCKLE analysis is carried out. Eigenvalues, also known as load multipliers, are extracted in this analysis and the lowest values are important. The buckling mode shapes are the most useful outcome in the eigenvalue analysis, since they predict the likely failure mode of the structure. In the analysis in this report, two buckling mode shapes were chosen. The first mode is normally an antisymmetric buckling shape whereas the second is normally symmetric. Buckling modes with both positive and negative signs are also considered in this study. Tables 1a, 1b and 1c show the buckling modes shapes of three test series: *V*-predominantly shear; *MV*-combined bending and shear; and *M*-bending only, respectively. Modes 1 are generally anti-symmetric about the centerline of the member, and Modes 2 are generally symmetric.
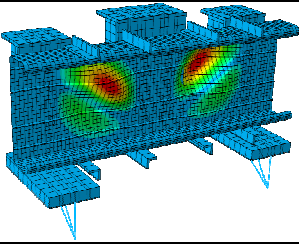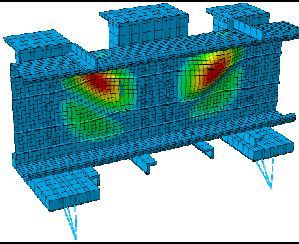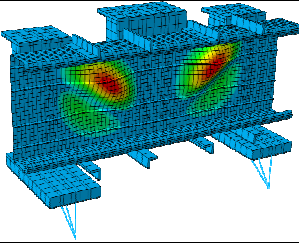
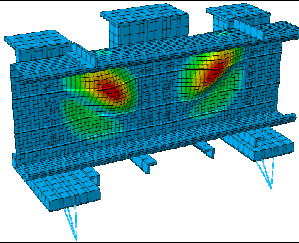Table 1a. Buckling Modes of *V* –Shear Test Series

V-Series	With Straps	Without Straps
Mode 1		
Mode 2		

Table 1b. Buckling Modes of *MV* – Combined Bending and Shear Test Series
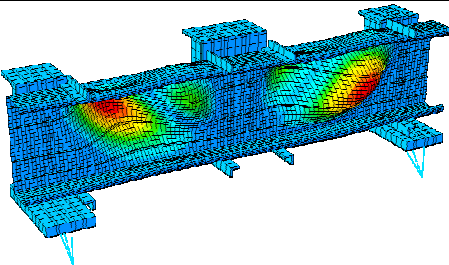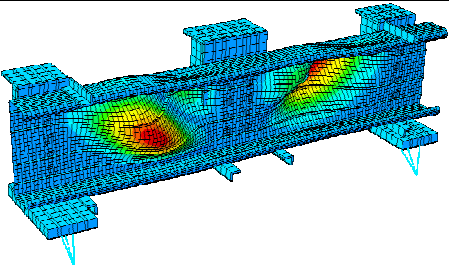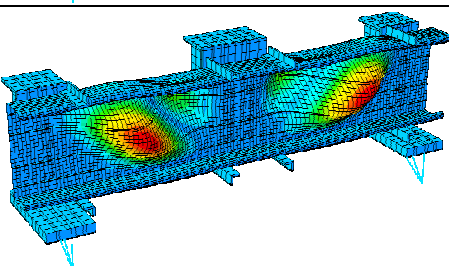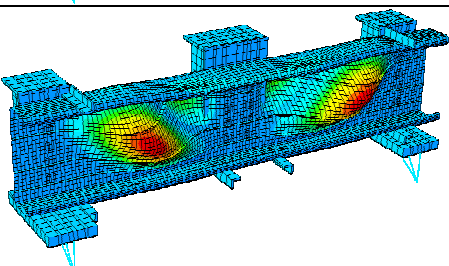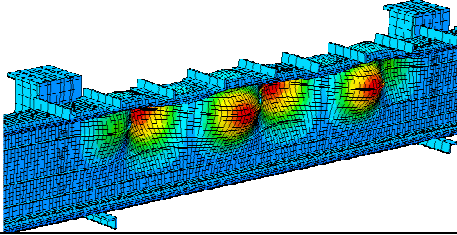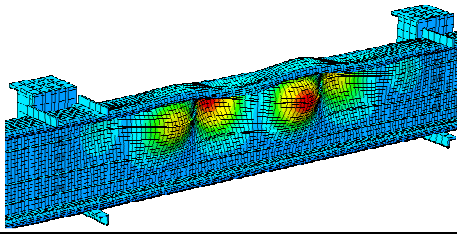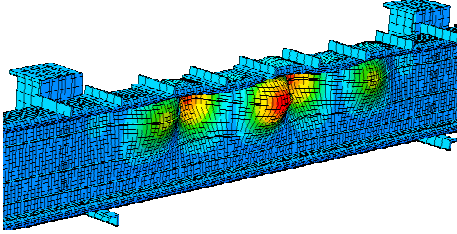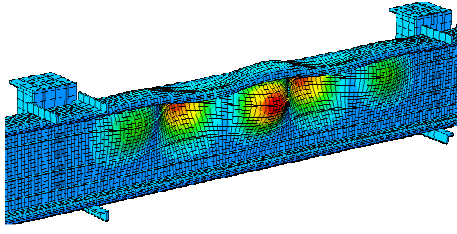
MV-Series	With Straps	Without Straps
Mode 1		
Mode 2		

Table 1c. Buckling Modes of *M* –Bending Only Test Series

MV-Series	With Straps	Without Straps
Mode 1		
Mode 2		

A structure which has material and geometrically nonlinearity or unstable postbuckling response requires a load-displacement analysis to be performed. This analysis is known as the "Modified Riks Method" and generally used to predict unstable, geometrically nonlinear collapse of a structure. The Riks method uses the load magnitude as an additional unknown; it solves simultaneously for loads and displacements. ABAQUS uses the "arc length" along the static equilibrium path in load-displacement space to measure the progress of solution. This method provides solutions regardless of whether the response is stable or unstable. Riks (1972, 1979) proposed an incremental approach to deal with the buckling and snapping problems. The Riks method works well in snap-through problems in which the equilibrium path in load-displacement space is smooth and does not branch. The Riks method can also be used to solve post-buckling problems both with stable and unstable post-buckling behaviour. However, the exact post-buckling problem cannot be analysed directly due to the discontinuous response at the point of buckling. To analyse this problem, the model has to have a continuous response instead of bifurcation. This effect can be accomplished by adding initial imperfections to create a perturbed mesh. There is therefore some response in the buckling mode before the critical load is reached. Herein, the *STATIC, RIKS procedure was used to perform the collapse or post-buckling analysis.

SOLUTION CONTROL PARAMETERS

The convergence and integration accuracy are very important factors in the finite element analysis, especially for simulation of thin sections with large displacement. In ABAQUS, there are many control parameters which are normally assigned by default values. However, in the analysis of very thin sections with large vertical displacements such as the *M* test series for bending only, a big problem with convergence has occurred. To solve this problem, the control parameters have to be adjusted in the *CONTROL option within a step definition. The main parameters which are adjusted in ABAQUS model are the I_0 for specifying the equilibrium iteration for a residual check and the I_R for specifying the equilibrium iteration for a logarithmic rate of convergence check. Both I_0 and I_R are adjusted to 10 and 12 respectively in this analysis. With these changes, convergent solutions can be obtained. In some cases, the adjustment of the parameters in the *STATIC, RIKS option can avoid divergence.

ELEMENT MESH AND TYPES

Element Mesh

Four differents mesh sizes were considered. The element sizes were 30 mm, 15 mm, 8 mm and 4 mm. The *MV*-combined bending and shear test of the SC20024 section was chosen to investigate the effect of mesh sizes on the accuracy and time-consumption of the analysis. The total numbers of elements including those of test rig are 2398, 4022, 8592 and 25842 elements respectively. Table 2 shows the results of the FE runs, number of elements, peak loads and CPU time of three different mesh sizes of the *MV*- combined bending and shear test of the SC20024 section.

Table 2. Influence of the Mesh Size

Mesh	Element Size (mm)	Number of Elements	Peak Load (kN)	CPU Time (s)
1	30x30	2398	335.538	218.4
2	15x15	4022	328.284	367.5
3	8x8	8592	325.43	804.2
4	4x4	25842	319.194	2892.6

All FE runs were performed on a Dell Optiplex GX520 workstation with Pentium (R) D CPU 3.40 GHz and 0.99 GB of internal memory. The CPU time needed to complete the run was chosen as a representative proportional indication of the total amount of time needed for completion. It should be noted that the total time is however an order of magnitude larger than the CPU time due to comparatively time-consuming input/output operation to disk.
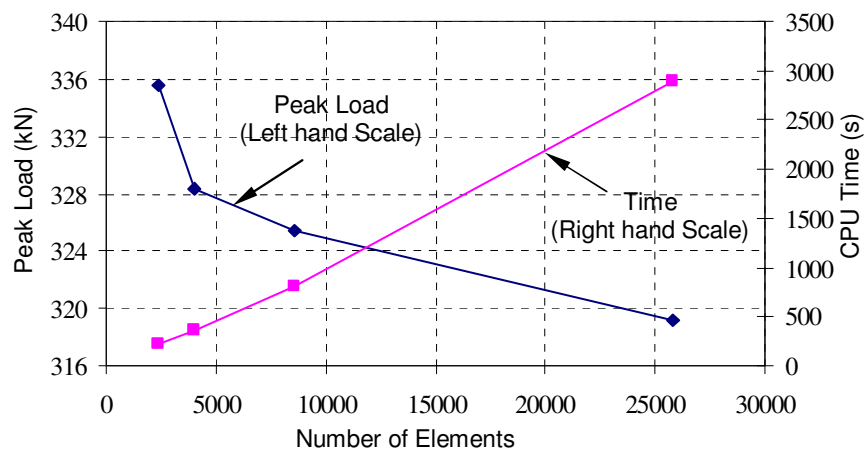

Figure 6. Effect of the Mesh Size on Peak Load and CPU Time

As can be seen in Fig. 6, as the mesh size decreases from 30 mm to 15 mm, the peak load drops dramatically from 335.538 kN to 328.284 kN. When the mesh is further refined to 8mm and 4 mm, the peak load converges asymptotically and has a little gain in accuracy to 325.43 kN and 319.194 kN respectively. Regarding the CPU time, when mesh size reduces from 8 mm to 4 mm, the CPU time increases significantly nearly 3.6 times from 804.2 s to 2892.6 s.

Fig. 7 displays the load-vertical displacement behaviour obtained for the different meshes. There is no noticeable difference in the results of the 8 mm and 4 mm element meshes well into the post-peak range and then there is slight difference after peak loads between these two meshes. This difference becomes irrelevant in practice. By comparison, the load-vertical displacement curves of the 15 mm and 30 mm element meshes lie significantly above the other two curves. So that, the results of such a coarse mesh size are then not accurate. Therefore, the 8 mm element mesh was selected for the numerical simulation. The peak load difference is about approximately 2 %, while it is subtantially more computationally efficient. It also guarantees that the load-vertical displacement curve is accurately modeled.
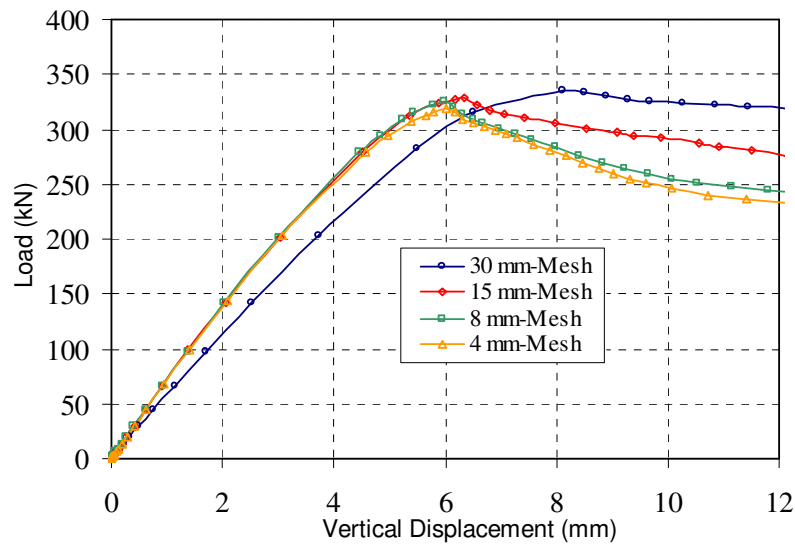
Figure 7. Load-Vertical displacement behaviours

Element Type

The 4-node shell element with reduced integration, type S4R, was selected from the ABAQUS element library. This element uses three translation and three rotational degrees of freedom at each node. The element accounts for finite membrane strains and arbitrarily large rotations. Therefore, it is suitable for large-strain analyses and geometrically nonlinear problems. The other elements with five degrees of freedom such as S4R5 can be more computationally economical. However, they cannot be used in finite-strain applications. According to the Simpson rule, reduced integration was carried out by using five integration points through the shell thickness. Since S4R is a linear element, the hourglass control settings needed to be activated.

The element type S4 is also modelled in comparison with the element type S4R. Element type S4 is a fully integrated, general-purpose, finite-membrane-strain shell element. The element's membrane response is treated with an assumed strain formulation that gives accurate solutions to in-plane bending problems, is not sensitive to element distortion, and avoids parasitic locking. Element type S4 does not have hourglass modes in either the membrane or bending response of the element; hence, the element does not require hourglass control.
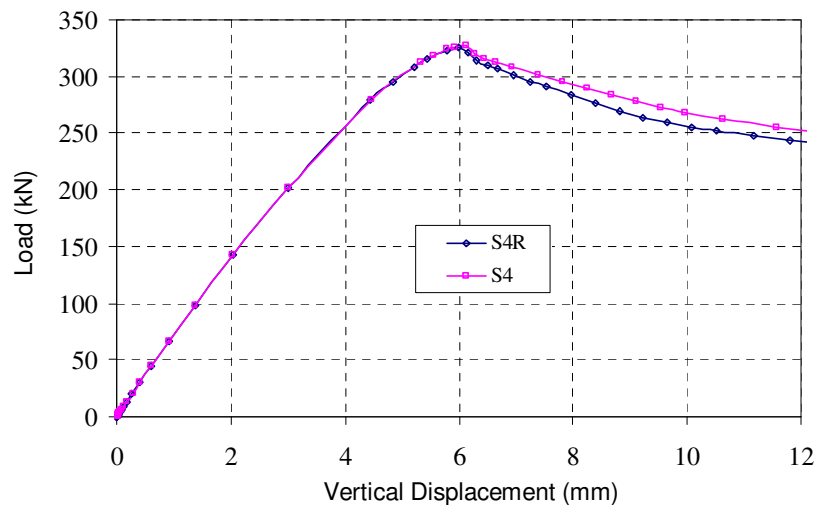
Figure 8. Effect of Reduced Integration

Fig. 8 shows load-vertical displacement behaviours of *MV-* combined bending and shear test of SC20024 sections with both S4R and S4 element types. Two curves are well-matched up to peak load. The difference at peak loads is not significant. After peak, the S4 curve lies slightly above the S4R. This is not significantly important in practice. The S4 element has four integration locations per element compared with one integration location for S4R, which makes the element computationally more expensive. Therefore, the element type S4R was selected for modeling all analyses in this report.

COMPARISONS OF TEST LOADS WITH FINITE-ELEMENT MODELLING

The results of the test and ABAQUS ultimate loads are given in Appendices 1-3. The ratios of mean test (P_T)/ABAQUS load are reproduced in Table 3a, 3b and 3c for the *V* – shear test series; *MV* – combined bending and shear test series ; and *M* – bending only test series respectively. The comparisons of the test and ABAQUS ultimate loads are also plotted against the buckling modes and geometric imperfections in Figs. 9-10, 16-17, and 23-24.

Table 3a. *V* – Shear Test Series and ABAQUS Results

Section V-Series	Test (P_T) (kN)	P_T/ABAQUS Load								
		Imp=0	Mode 1 0.15t	Mode 1 0.64t	Mode 1 -0.15t	Mode 1 -0.64t	Mode 2 0.15t	Mode 2 0.64t	Mode 2 -0.15t	Mode 2 -0.64t
V-SC15015	168.539	0.908	0.920	0.938	0.919	0.938	0.925	0.943	0.892	0.941
V-SC15015w	157.307	0.928	0.963	1.000	0.968	1.061	0.941	0.958	0.961	1.012
V-SC15019	222.317	0.966	0.985	1.017	0.980	1.018	1.006	1.032	0.943	1.008
V-SC15019w	207.484	0.973	1.001	1.075	0.999	1.054	1.054	1.024	1.017	1.069
V-SC15024	391.955	0.984	0.992	1.079	0.993	1.040	0.999	1.052	1.004	1.048
V-SC15024w	371.688	1.012	1.019	1.054	1.020	1.054	1.006	1.006	1.025	1.072
V-SC20015	185.936	0.946	0.950	0.956	0.945	0.958	0.947	0.942	0.952	0.962
V-SC20015w	182.212	1.011	1.042	1.056	1.041	1.064	0.964	0.973	1.057	1.074
V-SC20019	248.260	0.980	0.989	0.993	0.987	0.996	0.984	0.987	0.979	0.980
V-SC20019w	246.612	1.017	1.061	1.082	1.069	1.084	1.016	1.018	1.057	1.085
V-SC20024	496.826	1.039	1.068	1.101	1.068	1.101	1.058	1.093	1.013	1.053
V-SC20024w	469.235	1.037	1.076	1.117	1.069	1.142	1.045	1.081	1.068	1.126

Table 3b. *MV* – Combined Bending and Shear Test Series and ABAQUS Results

Section MV-Series	Test (P_T) (kN)	P_T/ABAQUS Load								
		Imp=0	Mode 1 0.15t	Mode 1 0.64t	Mode 1 -0.15t	Mode 1 -0.64t	Mode 2 0.15t	Mode 2 0.64t	Mode 2 -0.15t	Mode 2 -0.64t
MV-SC15015	117.873	1.014	1.069	1.102	1.074	1.094	1.010	1.018	1.051	1.065
MV-SC15015w	79.355	0.981	0.979	0.961	0.979	0.958	0.978	0.959	0.986	0.963
MV-SC15019	154.499	1.043	1.065	1.064	1.063	1.062	1.047	1.044	1.042	1.062
MV-SC15019w	118.178	1.033	1.055	1.049	1.032	1.046	1.031	1.029	1.036	1.035
MV-SC15024	256.196	0.996	0.997	1.002	0.997	1.002	0.992	0.999	0.997	1.001
MV-SC15024w	214.809	0.994	0.998	1.005	0.983	1.010	0.983	0.976	0.990	1.022
MV-SC20015	108.595	0.909	0.944	0.956	0.945	0.958	0.903	0.908	0.971	0.981
MV-SC20015w	83.262	0.979	0.988	0.977	0.983	0.982	0.985	0.963	0.980	0.980
MV-SC20019	166.707	0.952	0.978	0.994	0.979	0.996	0.957	0.960	1.003	1.065
MV-SC20019w	126.480	1.069	1.070	1.075	1.083	1.058	1.078	1.062	1.085	1.071
MV-SC20024	320.107	0.993	0.990	1.012	0.988	1.007	0.985	1.003	0.989	1.016
MV-SC20024w	244.781	0.994	0.997	1.040	0.996	1.016	0.983	0.960	1.010	1.027

Table 3c. *M* –Bending Only Test Series and ABAQUS Results

Section M-Series	Test (P_T) (kN)	P_T/ABAQUS Load								
		Mode 1 Imp=0	Mode 1 0.15t	Mode 1 0.64t	Mode 1 -0.15t	Mode 1 -0.64t	Mode 2 0.15t	Mode 2 0.64t	Mode 2 -0.15t	Mode 2 -0.64t
M-SC15015	40.960	0.987	1.050	1.134	1.049	1.135	1.041	1.119	1.044	1.121
M-SC15015w	32.780	0.892	0.899	0.968	0.901	0.967	0.886	0.948	0.900	0.966
M-SC15019	57.014	1.028	1.077	1.195	1.076	1.204	1.075	1.075	1.083	1.188
M-SC15019w	50.482	1.057	1.061	1.120	1.061	1.121	1.054	1.094	1.064	1.119
M-SC15024	105.970	1.133	1.155	1.261	1.156	1.262	1.161	1.251	1.164	1.257
M-SC15024w	94.189	1.104	1.096	1.179	1.093	1.180	1.088	1.163	1.058	1.166
M-SC20015	53.534	1.003	0.993	1.022	0.991	1.022	0.891	1.048	1.011	1.043
M-SC20015w	46.331	0.933	0.928	0.985	0.968	0.987	0.949	0.971	0.922	0.986
M-SC20019	82.408	1.014	1.083	1.159	1.083	1.161	1.094	1.179	1.101	1.183
M-SC20019w	68.490	0.965	0.964	0.992	0.967	1.015	0.961	1.013	0.961	1.012
M-SC20024	169.088	1.097	1.150	1.268	1.152	1.268	1.157	1.272	1.162	1.286
M-SC20024w	145.770	1.067	1.076	1.130	1.072	1.122	1.065	1.120	1.077	1.143

For *V* – shear test series, as can be seen in Fig. 9, the test loads with straps are comparable with ABAQUS results over both geometric imperfections of amplitude 0.15t and 0.64t. The differences in the results between ABAQUS and the tests are less than 10%. In the case of the antisymmetric Mode 1 with magnitude 0.15t, the ABAQUS results are in the best agreement with the test results. Although the zero imperfection results are also very good for this case, it is not however recommended to use zero imperfections as the nonlinear deformations may not be triggered. Fig. 10 shows similar comparisons to Fig. 9 except that it applies to the tests without the straps. The results are generally less accurate and more variable than the tests with the straps especially with imperfection magnitude of 0.64t. It appears that the imperfection of the top flange adjacent to the loading points obtained by buckling analysis causes the reduction of the ABAQUS results especially with a large imperfection magnitude of 0.64t. As can be seen in Fig. 10, the ABAQUS results with symmetric Mode 2 and imperfection magnitude of 0.15t give the best predictions on average in comparison with the tests.
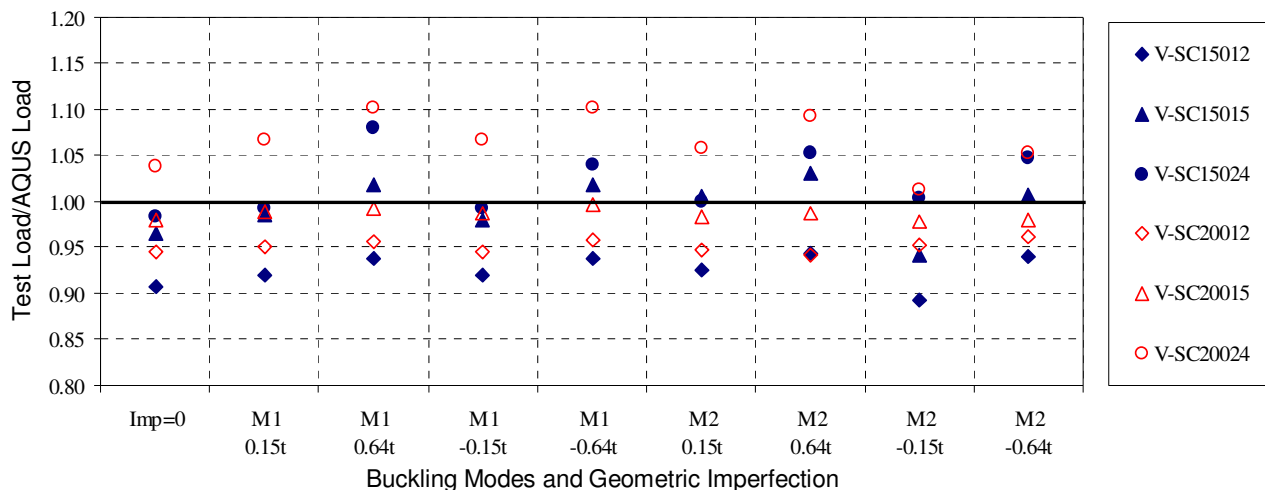

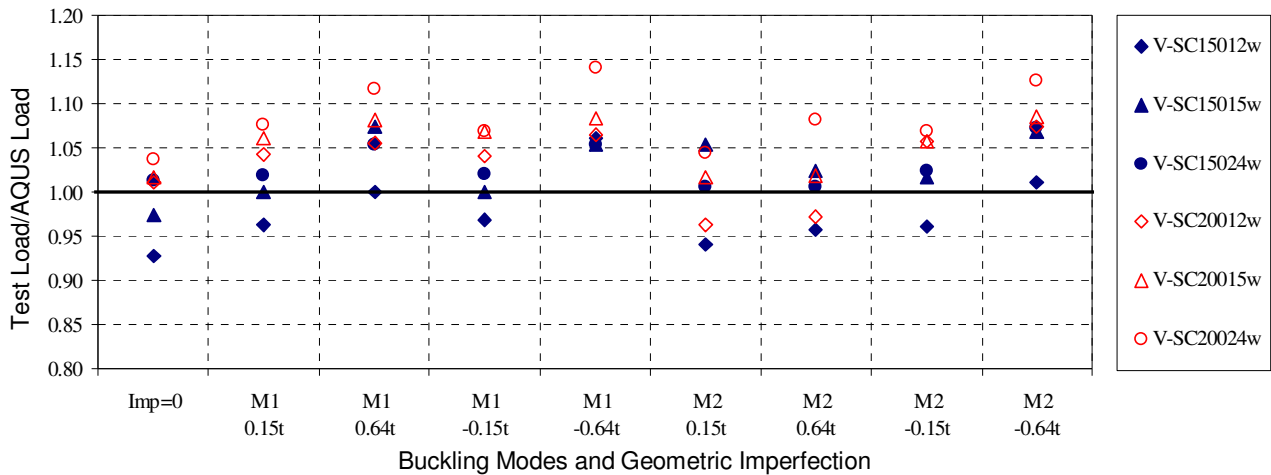Figure 9. Comparison of Test and ABAQUS Loads – V Series – With Straps

Figure 10. Comparison of Test and ABAQUS Loads – V Series – Without Straps
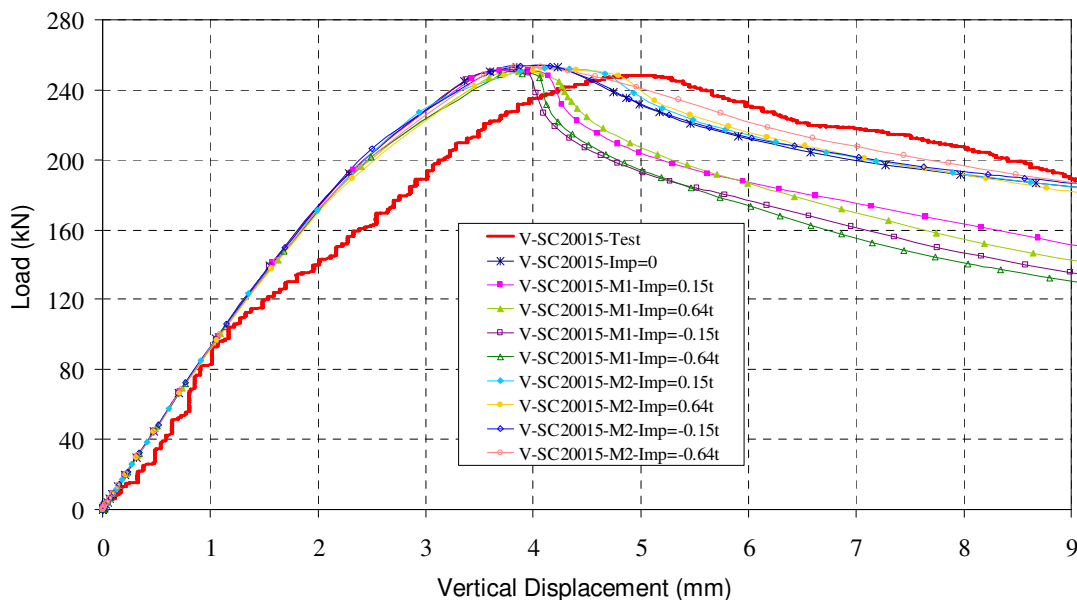

Figure 11. Load and Vertical Displacement Relations of V-SC20015 – With Straps

The load-vertical displacement curves for the *V* – shear test series with straps of the SC20015 section and ABAQUS results are illustrated in Fig. 11. When the load increases up to about 100 kN, the load increases linearly and matches with that of the ABAQUS model. The explanation is due to the contacts between the channel members and the test rig. In the test, two beam specimens were bolted through the webs by vertical rows of M12 high tensile bolts. These rows of bolts were then connected to two channel sections 250x90x6CC with stiffeners. All M12 high tensile bolts of 830 MPa for Grade 8.8 were pretensioned up to 90 kNm torque to prevent slip under initial loading. In the ABAQUS model, the "tie" constraints were used to model contacts between the specimens and rig at the locations of the bolts as shown in Fig. 5(b). However, when the same loads increase from 100 kN to their peak, the test curve deflections are associated with higher displacements in comparison with the ABAQUS models. The loads are greater than the friction caused by pretension of the high strength bolts. Further displacement is due to the slip between the beam specimens and the test rig which is difficult to model in ABAQUS. At the peak load, the vertical displacement of ABAQUS model is about 4 mm, whereas it is roughly about 5 mm in the test. Apart from the slip, the bearing capacity of the beam channel at the holes where the high strength bolts acted also causes additional deflection. Especially, for *V* – shear test series, the structural members are quite "stiff" so that the high loads which are needed to obtain ultimate failure will cause local bearing failure. Fig. 12 shows the bolt slip and local bearing failure at holes which cause additional deflection as explained above.
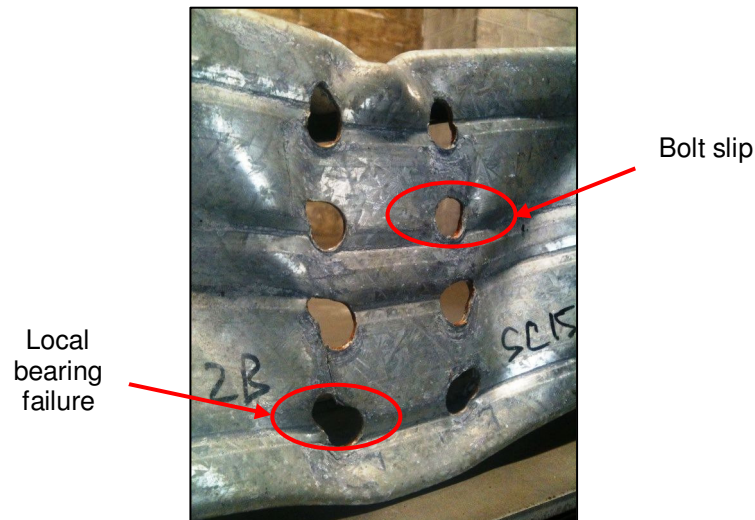
Figure 12. Bolts Slip and Local Bearing Failure at Holes

After the peak load in the ABAQUS model, the curves with Mode 1 imperfection where the buckling mode is antisymmetric drop more sharply than those with Mode 2 symmetric imperfection. It can be explained by the stress redistribution at only one span of the V – shear test which causes failure mode in 1 span only. Fig. 13 shows the corresponding failure mode shapes of V – shear test with straps of the SC20015 section for the test and ABAQUS model. The failure modes are identical and symmetrical for both test and ABAQUS. As can also be seen in Fig. 11, soon after the peak load, the load-vertical displacement curve of the test is of the same shape as the ABAQUS curves with Mode 2 symmetric imperfection.
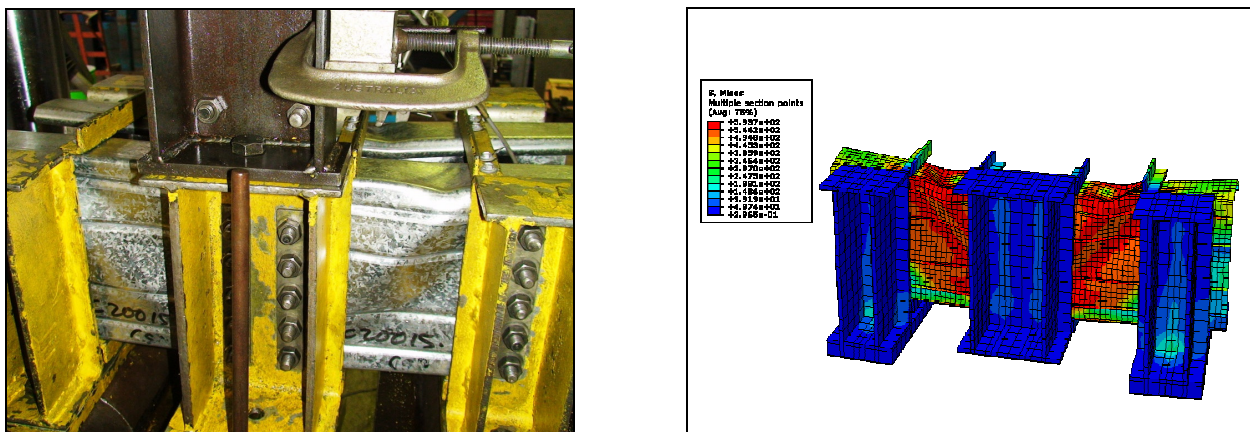
Figure 13. Failure Mode Shapes of Test and ABAQUS Model of V-SC20015-With Straps

Fig. 14 shows the load-vertical displacement curves for the V – shear test series without the straps for the SC20015 section and the ABAQUS results. For the test, there are additional deflections up to about 5 kN compared with ABAQUS. The reason is due to the test assembly. The two load transfer plates did not rest evenly on the half rounds because of slight twist after assembly. The load is then fairly matched with ABAQUS up to 100 kN. After this point up to peak load, the bolts start to slip and lead to the further increase in the displacements of test in comparison with that of ABAQUS. The explanation is the same as above due to slip and local bearing failure.
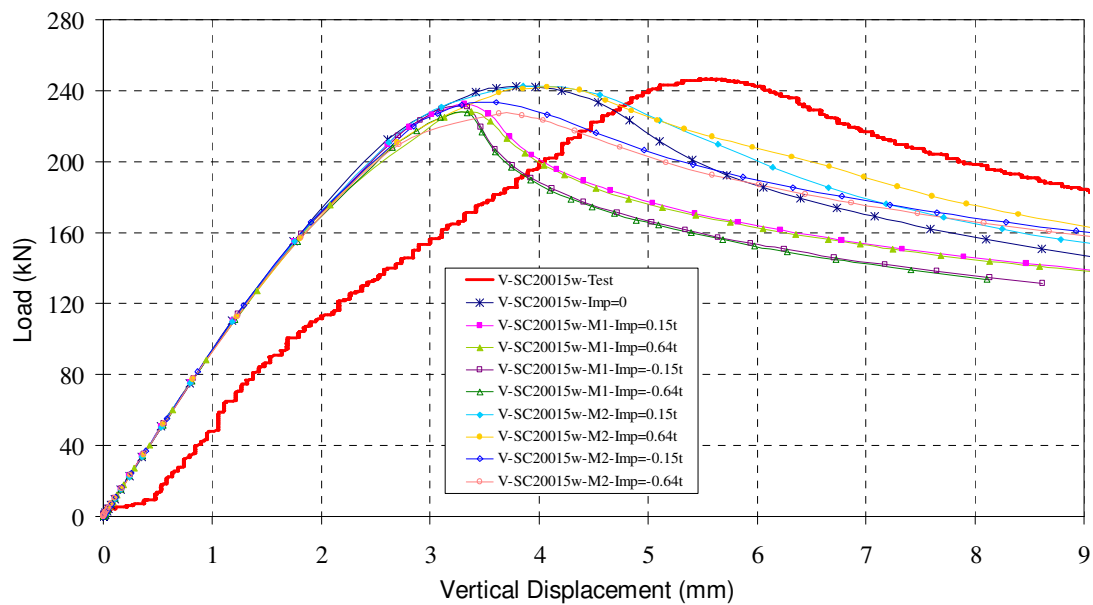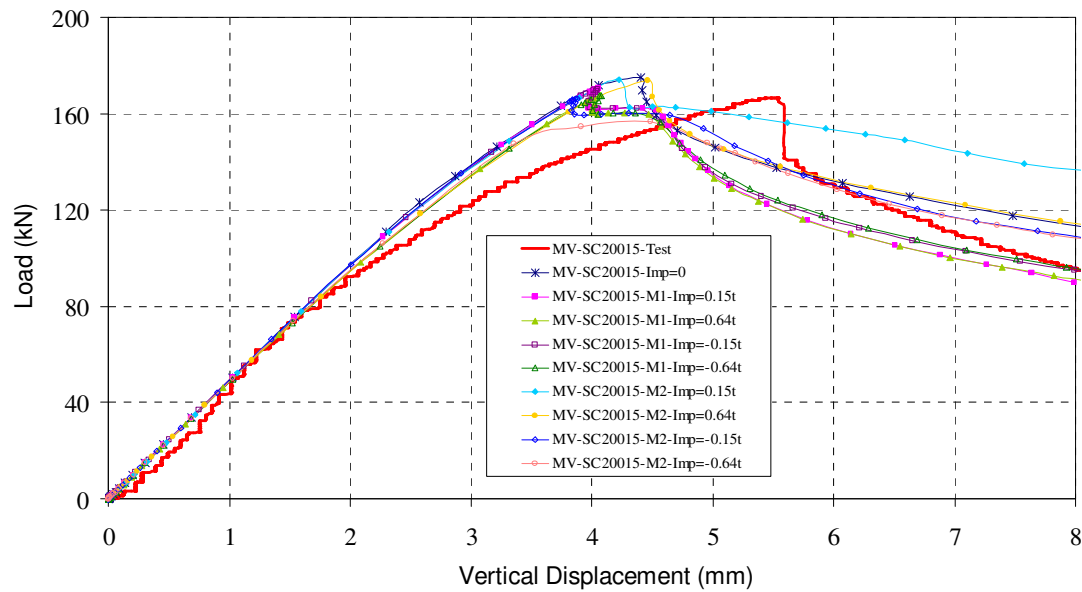
Figure 14. Load and Vertical Displacement Relations of V-SC20015 – Without Straps
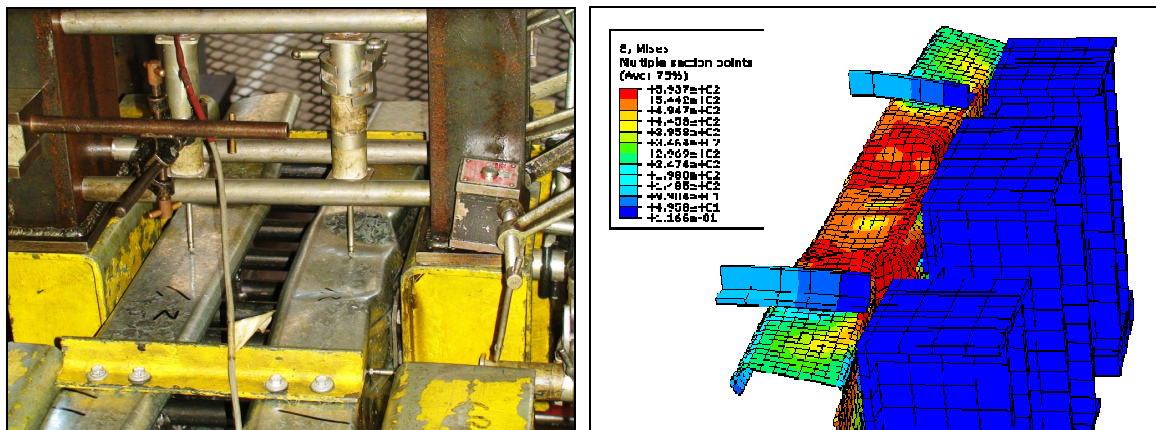
Figure 15. Failure Mode Shapes of Test and ABAQUS Model of V-C20019-Without Straps

As can also be seen in Fig. 15 which shows the corresponding failure mode shapes of the *V* – shear test without the straps of the SC20015 section for the test (left hand specimen) and ABAQUS model. The failure occurs in both spans which is matched with the ABAQUS model where Mode 2 symmetric imperfection was used. The load-vertical displacement curve of the test after peak load is similar to the ABAQUS model with Mode 2 symmetric buckling mode.

For the *MV* - combined bending and shear test series, Figs. 16-17 show the comparisons between the tests and ABAQUS results in cases with and without straps respectively. The ABAQUS results are generally in good agreement with the test results. The difference of results between ABAQUS and tests are less than 10% for both cases. It is interesting to note that the ABAQUS results for large imperfection magnitude of 0.64t are not significantly lower than those of 0.15t. This shows that the results of ABAQUS are not significantly sensitive to the initial imperfections for the *MV* - combined bending and shear test series.
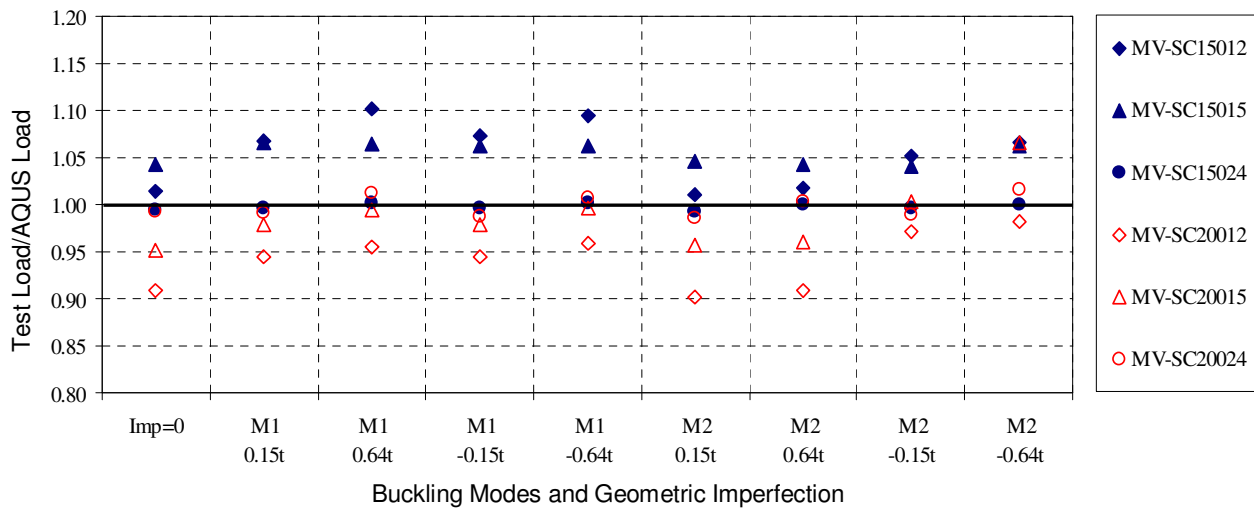
Figure 16. Comparison of Test and ABAQUS Loads – MV Series – With Straps
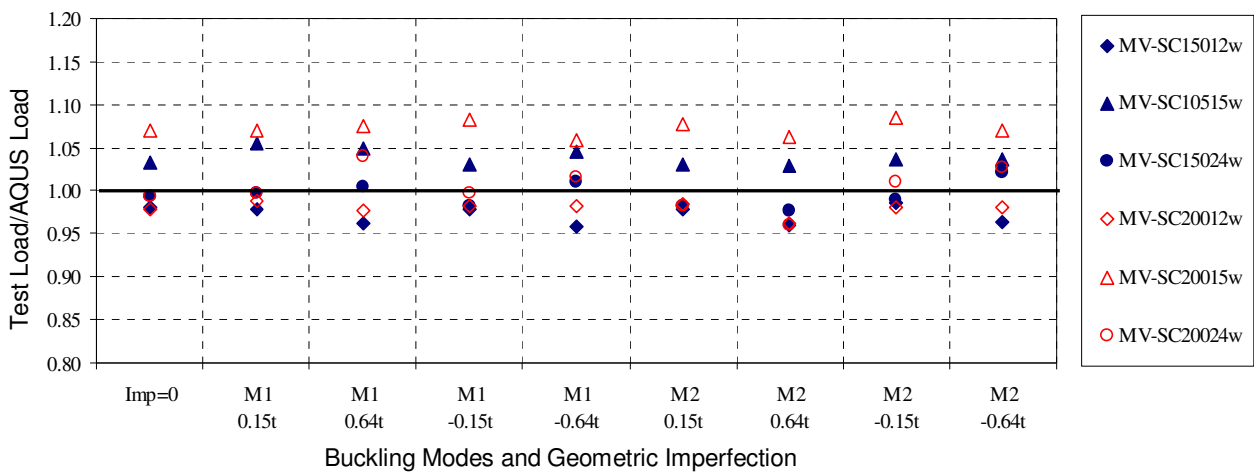
Figure 17. Comparison of Test and ABAQUS Loads – MV Series – Without Straps

Fig. 18 shows the load-vertical displacement curves for the *MV* - combined bending and shear test series with straps for the SC20015 test sections and the ABAQUS results. The ABAQUS results show a similar trend to the test results when loads increase up to 100 kN. The reason for this is due to the fact that the pretension of high strength bolts avoids slip between channel members and test rig. As the load keeps increasing to the peak load, the vertical displacements of the tests are greater than those of the ABAQUS model. The explanation is mainly a result of slip and elongation of holes caused by local bearing capacity of channel ply. After the peak, as can be seen in Fig. 19 which shows the corresponding failure mode shapes of *MV* - combined bending and shear test with the straps for the SC20015 section for test and ABAQUS models, the failure occurs in the left hand span only which is matched with the ABAQUS model where Mode 1 antisymmetric imperfection was used. The load-vertical displacement curves for the tests after the peak loads are similar to the ABAQUS model with the Mode 1 antisymmetric buckling mode.

School of Civil Engineering
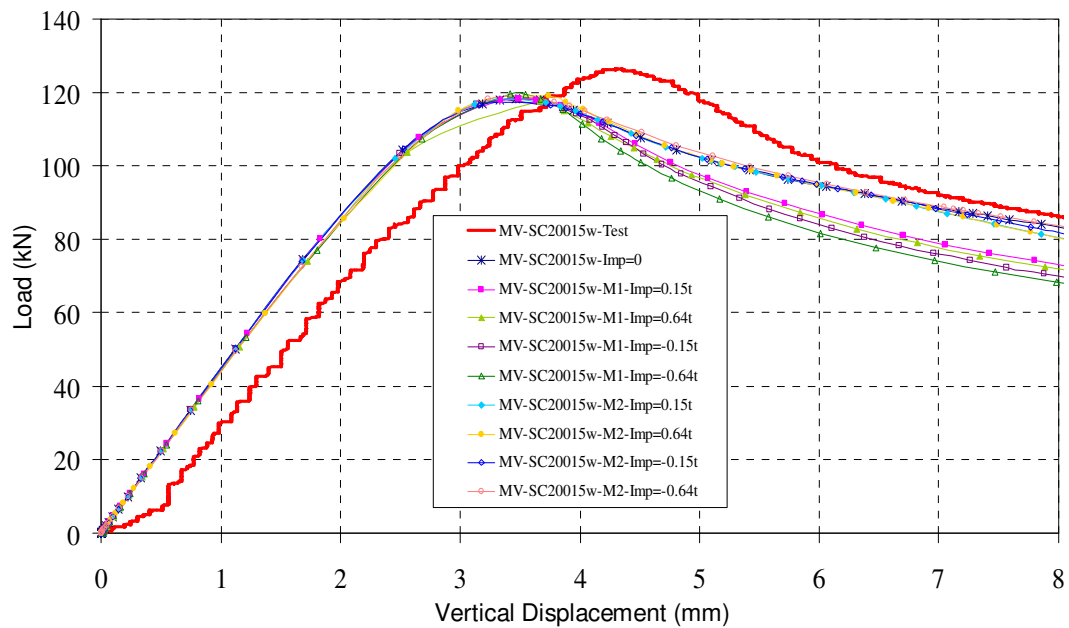The University of Sydney
    Research Report R913
    Page 19

Figure 18. Load and Vertical Displacement Relations of MV-SC20015 – With Straps
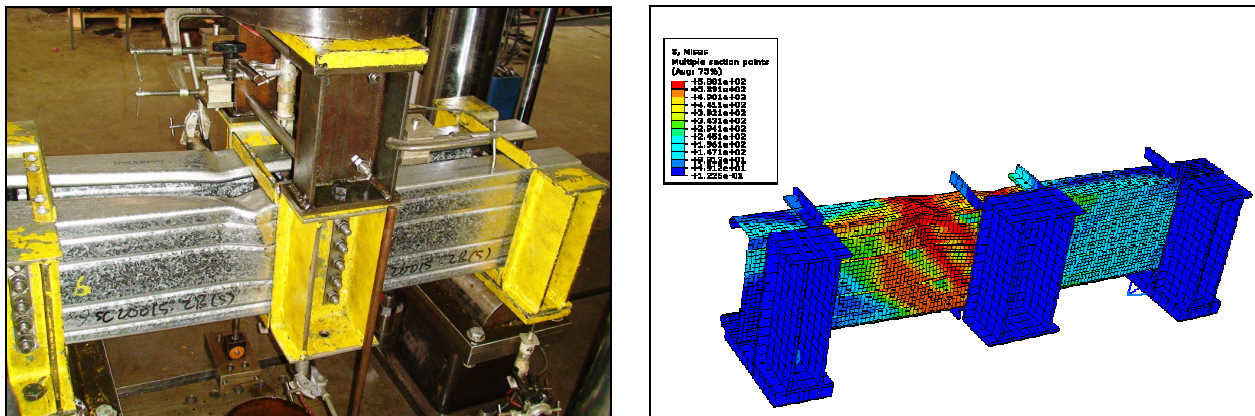
Figure 19. Failure Mode Shapes of Test and ABAQUS Model of MV-SC20015-With Straps

To further understand the stress development in the ABAQUS model for SC20015 channel section member under *MV* - combined bending and shear test with straps, Fig. 20 shows the FE deformations of SC20015 *MV* - combined bending and shear test with straps under progressive loading through six images which correspond to the points in the accompanied load vs vertical displacement graph. The contours represent Von Mises surface stress. From different views, it can be seen at point (3) that the highest membrane stresses are developed at mid span between two rows of bolts in pure bending region. There is little drop at point (3) as shown in the load vs vertical displacement graph. This shows that the channel has buckled at midspan. However, the load does not drop significantly but keeps almost the same whereas the stresses are developed at the diagonal on left hand span due to combined bending and shear as shown at point (4). The channel then fails at the web and then the flange. This shows the dramatic drop at point (5) as shown in load vs vertical displacement graph. After this point, the load-vertical displacement curve of the ABAQUS model, using Mode 1 antisymmetric buckling mode imperfection, is similar to the test. Failure only occurs in one span as shown in Fig. 19.

(1)-Initial

(2)-Before-Peak

(3)-Peak

(4)-Post-Peak

(5)-Post-Peak

(6)-Post-Peak
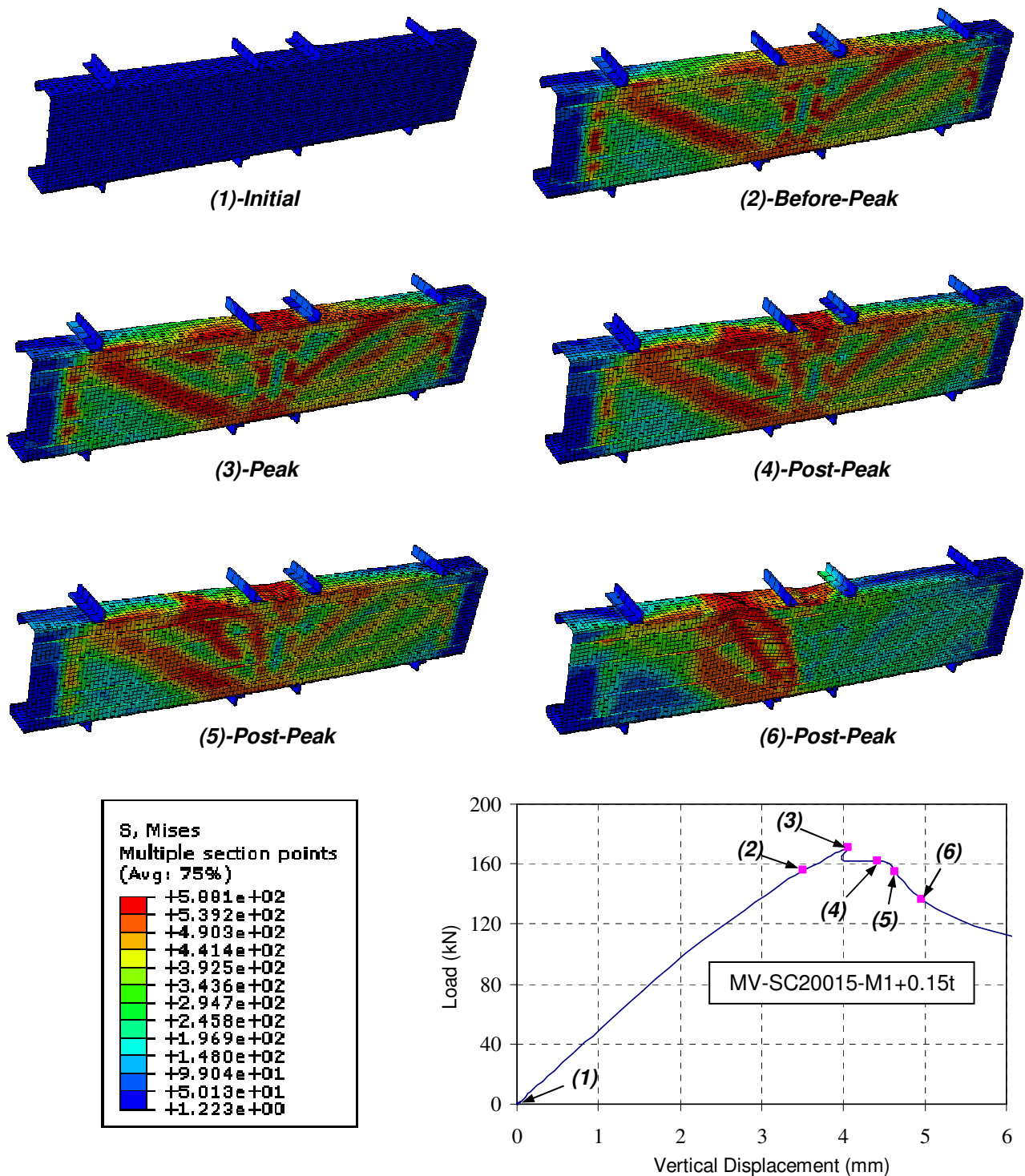
Figure 20. Deformations under Progressive Loading of SC20015 Section, *MV* - Combined Bending and Shear Test Series-with Straps

Fig. 21 shows the load-vertical displacement curves for the *MV* - combined bending and shear test series without the straps for the C20019 section and the ABAQUS results. Peak loads are well predicted by the ABAQUS modeling. It can be seen that before the peak load, the test curves increase further than the ABAQUS model because of the same explanation of slip and elongation of the holes as before. After the peak, it can be seen in Fig. 22 which shows the corresponding failure mode shapes of *MV* - combined bending and shear test without straps of C20019 section for test and ABAQUS model, the buckling shape is the same as that of test where failure occurs in one span.

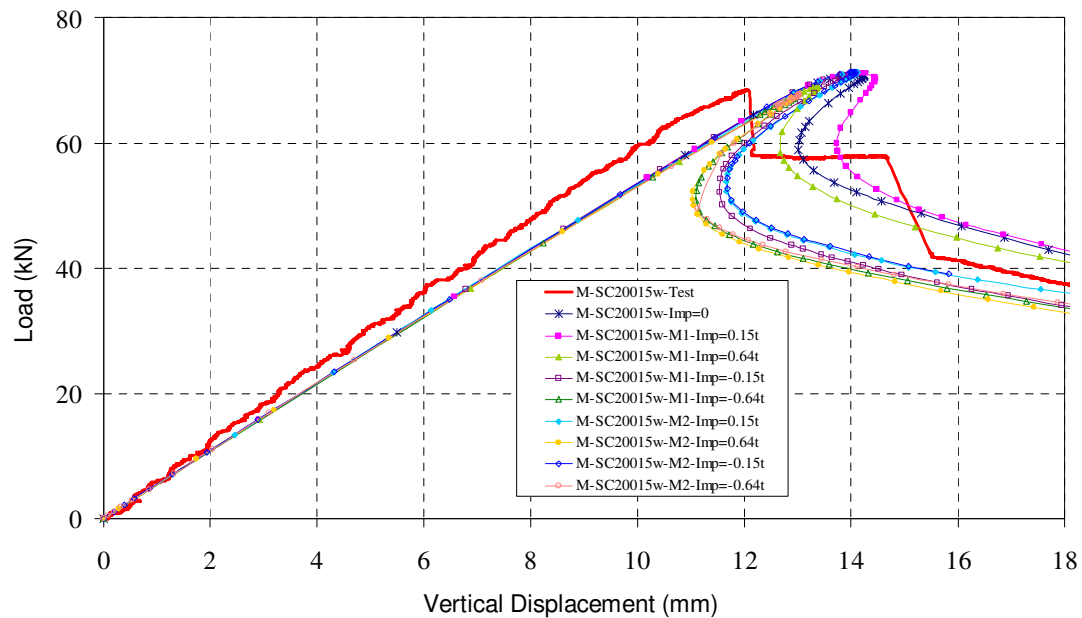Figure 21. Load and Vertical Displacement Relations of MV-SC20015 – Without Straps
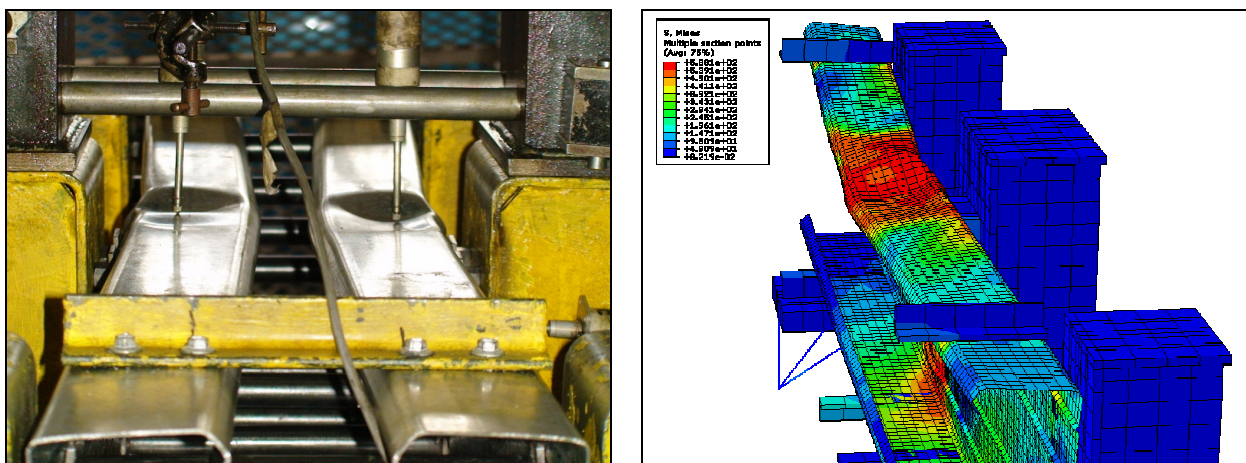
Figure 22. Failure Mode Shapes of Test and ABAQUS Model of MV-C20019-Without Straps

For the *M* - bending only test series, Figs. 23-24 show the comparisons between the tests and ABAQUS results in the cases with and without the straps respectively. When the geometric imperfection magnitude is 0.15t, the ABAQUS results are generally in good agreement with the test results and the differences of the results are about 10% for both with and without. However, the ABAQUS results are significantly sensitive to greater imperfections of 0.64t for the *M* - bending only test series. Especially, for tests with straps, the results are more variable and scattered. The differences of the results between ABAQUS and the tests are up to 30 %. For the tests without the straps, the differences are less severe but still up to 20%.
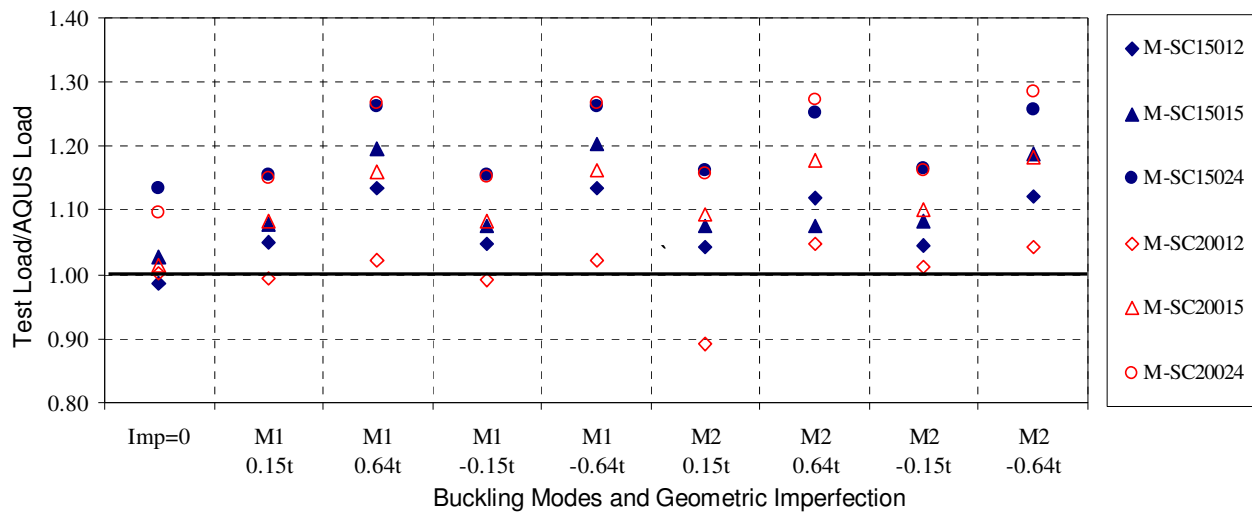
Figure 23. Comparison of Test and ABAQUS Loads – M Series – With Straps
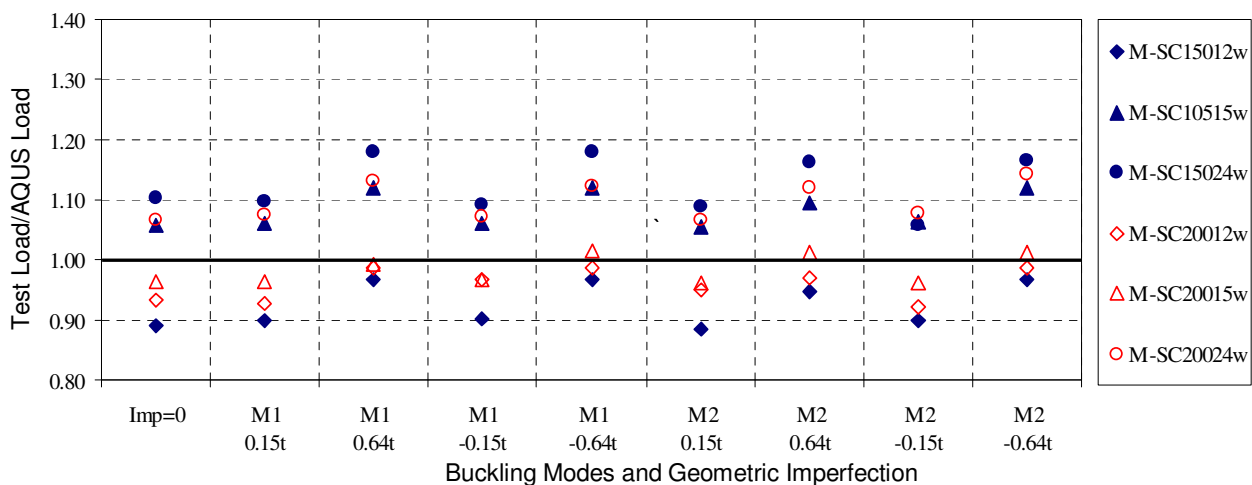
Figure 24. Comparison of Test and ABAQUS Loads – M Series – Without Straps

As can be seen in Figs. 25-26 which show load-vertical displacement curves for the *M* – bending test series both with and without straps for the SC20015 section and ABAQUS results, the test loads match well with the ABAQUS results up to the peak load. The ultimate loads are not as large as those of *V* – shear test series and *MV* – combined bending and shear test series. This shows that the structure in *M* – bending test is not as "stiff" as that of *V* – shear test series and *MV* – combined bending and shear test series. There is a small slip or elongation of the hole. This explains the good match between the tests and ABAQUS results up to the peak load. It is interesting to note that the test load drops twice in the load-vertical displacement curve graphs. The reason is due to the fact that the channel section members were tested in pairs and one channel failed before the other. As can also be seen in Figs. 25-26 after the two channels fail, the load-vertical displacement curves are of the same shape as those of the ABAQUS model with Mode 1 antisymmetric buckling mode. Figs. 27-28 show the corresponding failure mode shapes for the *M* - bending tests both with and without straps for the SC20015 section for the tests and ABAQUS models. All the buckling shapes are the same as those of tests.
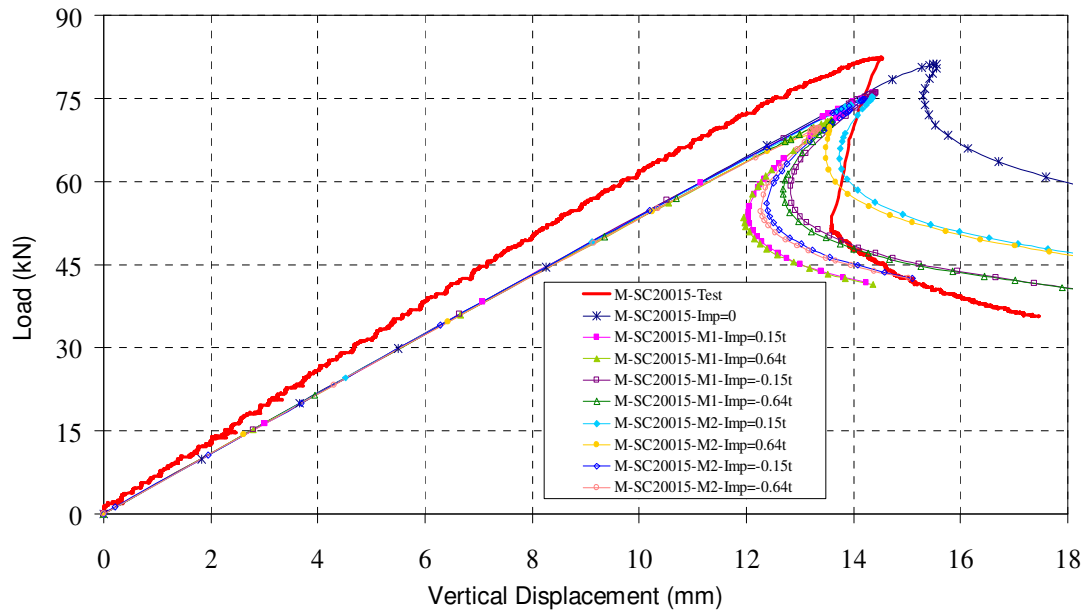
Figure 25. Load and Vertical Displacement Relations of M-SC20015 – With Straps

Figure 26. Load and Vertical Displacement Relations of M-SC20015 – Without Straps
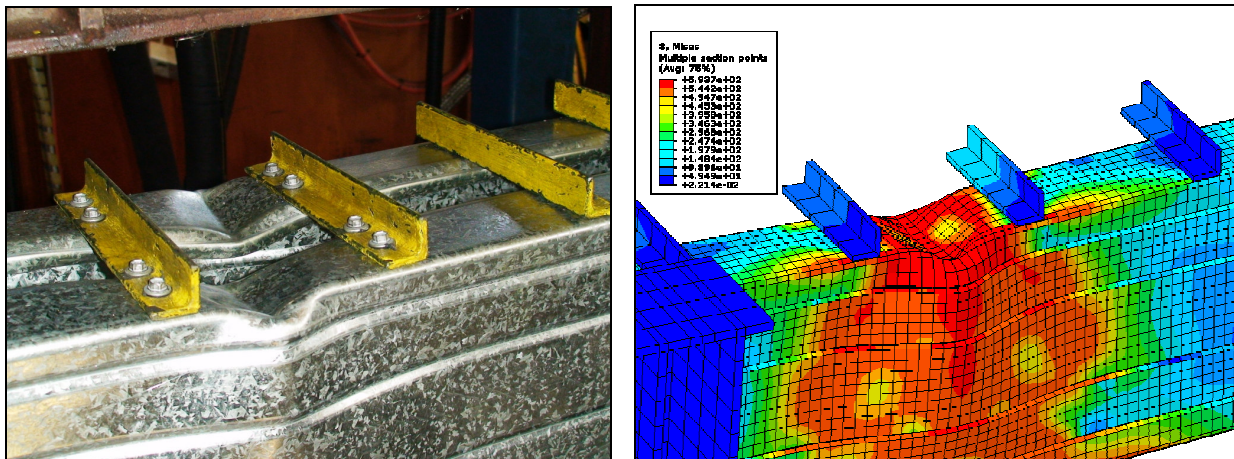
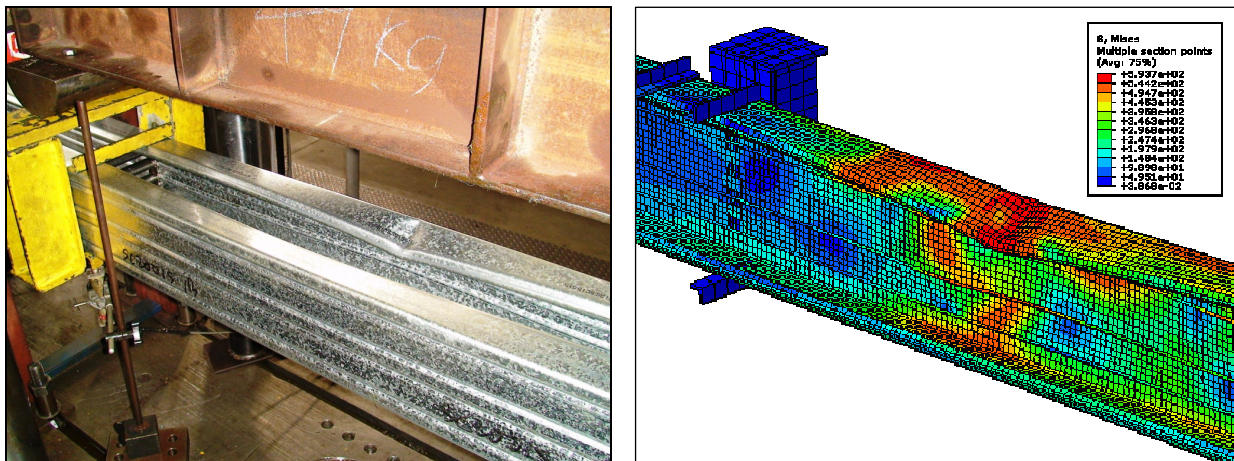Figure 27. Failure Mode Shapes of Test and ABAQUS Model of M-SC20015-With Straps

Figure 28. Failure Mode Shapes of Test and ABAQUS Model of M-SC20015-Without Straps

CONCLUSION

A series of ABAQUS simulations was carried out on high strength SupaCee® section cold-formed steel purlins. The simulations are compared with and calibrated against three different test series on high strength cold-formed C-section purlins which include predominantly shear *(V)*, combined bending and shear *(MV)* and bending only *(M)* test series of two different section depths and three different thicknesses of lipped channel section. The FE study was conducted for different effects of such input parameters as initial geometric imperfection, element type and the size of element mesh. Two scaling factors of 0.15t and 0.64t with both positive and negative signs where t is the thickness of channel section were used for initial geometric imperfection input. The use of the FE program ABAQUS for simulating the behavior of high strength SupaCee® section cold-formed purlins is successful since the ABAQUS results were generally in good agreement with experimental values. FE results show that the effect of initial geometric imperfection is not significantly sensitive for *V*-predominantly shear and *MV*-combined bending and shear test series. For *M*-bending only test series, the FE results are in good agreement with small imperfection of 0.15t but are more variable and scattered with larger imperfection of 0.64t because of the sensitization in the initial geometric imperfection. ABAQUS can therefore be used for further investigation to design and optimize thin-walled sections of high strength steel.

REFERENCES

ABAQUS/Standard Version 6.8-2; Abaqus/CAE User's Manua,. (2008), Dassault Systèmes Simulia Corp., Providence, RI, USA.

Camotim, D. and Silvestre, N. (2004). "GBT-based Analysis of The Distortional Postbuckling Behaviour of Cold-formed Steel Z-section Columns and Beams", *Proceedings of Fourth International Conference on Thin-Walled Structures*, Loughborough, pp. 243-250.

Hibbitt, Karlsson, and Sorensen, Inc. (HKS) (1997). *ABAQUS/Standard user's manual, Version 5.7.*

LaBoube, R. A., and Yu, W. W. (1978). "Cold-Formed Steel Web Elements under Combined Bending and Shear.", *Proc., 4th Int. Specialty Conf. on Cold-Formed Steel Structures*, University of Missouri-Rolla, St Louis, Missouri, U.S.A.

Lysaght (2003). "NSW SupaCee® is trademark of Bluescope Steel Limited." *Bluescope Steel Limited trading as Bluescope Lysaght.*

Pham, C. H. and Hancock, G. J. (2009). "Experimental Investigation of High Strength Cold-Formed C-Section in Combined Bending and Shear", *Research Report No R894*, School of Civil Engineering, The University of Sydney, NSW, Australia, April, 2009.

Pham, C. H., and Hancock, G.J. (2010a). "Numerical Simulation of High Strength Cold-Formed Purlins in Combined Bending and Shear", *Journal of Constructional Steel Research*, Volume 66, No 10, pp. 1205-1217.

Pham, C. H. and Hancock, G. J. (2010b). "Experimental Investigation of High Strength Cold-Formed SupaCee® Section in Combined Bending and Shear", *Research Report No R907*, School of Civil Engineering, The University of Sydney, NSW, Australia, January, 2010.

Riks, E. (1972). "The Application of Newton's Method to The Problem of Elastic Stability", *Journal of Applied Mechanics*, Vol 39, pp. 1060-1066.

Riks, E. (1979). "An Incremental approach to The Solution of Snapping and Buckling Problems", *International Journal of Solids Structures*, Vol 15, pp. 529-551.

Schafer, B. W. and Peköz, T. (1998). "Computational modeling of cold-formed steel: characterizing geometric imperfections and residual stresses", *Journal of Constructional Steel Research*, Vol 47, pp. 193-210.

Yang, D., and Hancock, G. J. (2006). "Numerical Simulation of High-Strength Steel Box-Shaped Columns Failing in Local and Overall Buckling Modes.", *Journal of Structural Engineering*, American Society of Civil Engineers, Vol 132, Issue 4, pp. 541-549.

Yu, C. (2005). "Distortional Buckling of Cold-Formed Steel Members in Bending.", *Ph.D. Dissertation*, Johns Hopkins Univ., Baltimore.

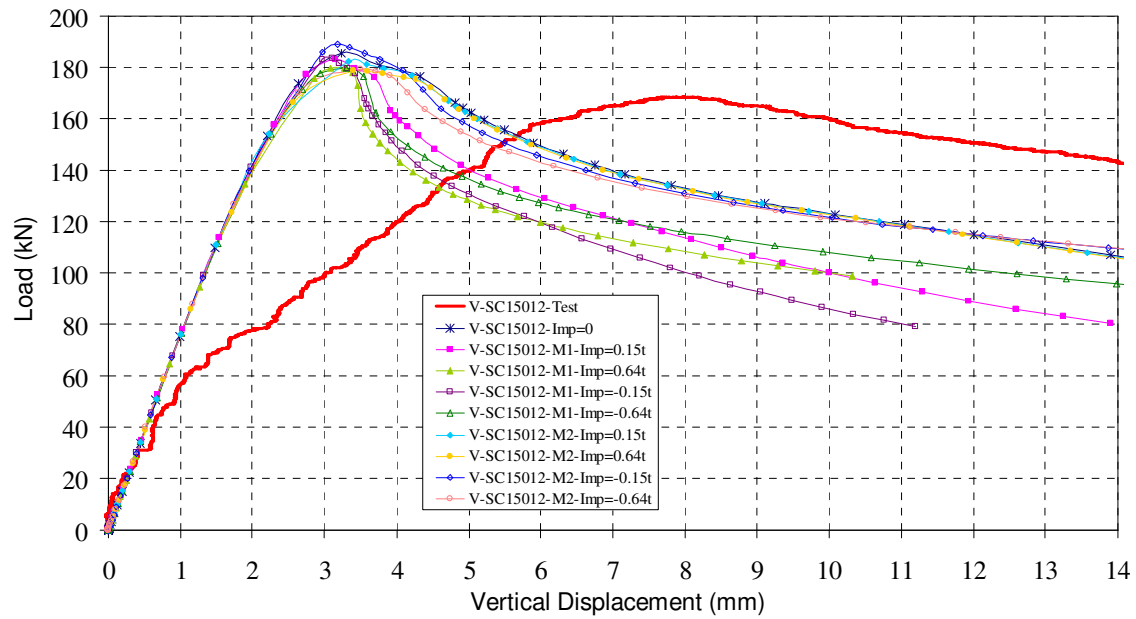**APPENDIX 1: FIGURES-TEST VERSUS FEM DISPLACEMENTS (FOR ALL TESTS)**

Figure 29. Load and Vertical Displacement Relations of V-SC15012 – With Straps
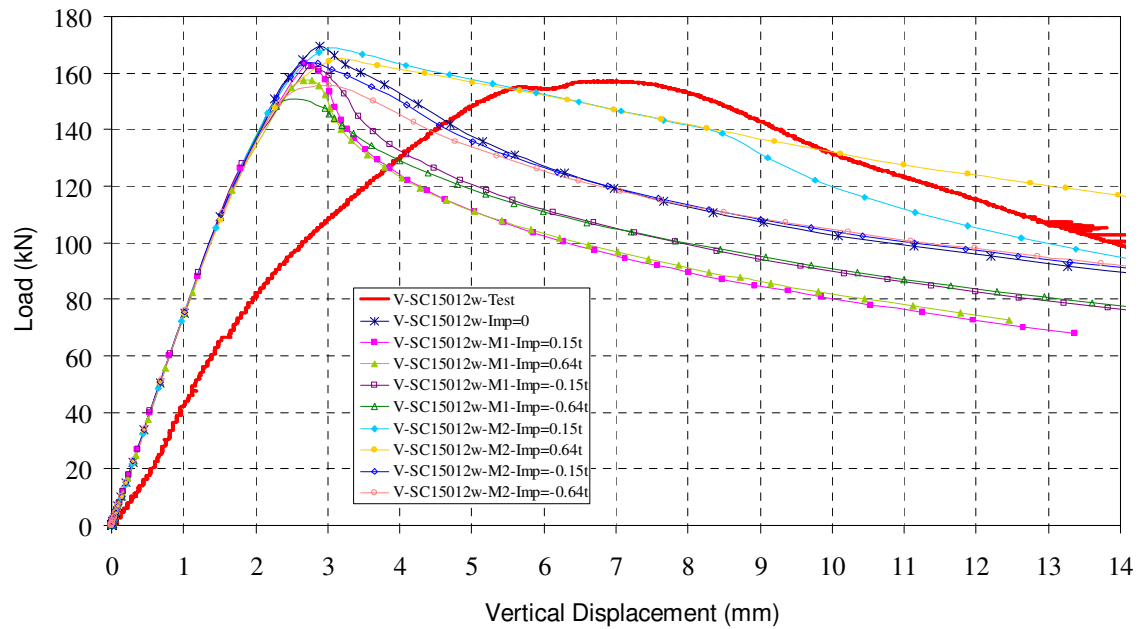

Figure 30. Load and Vertical Displacement Relations of V-SC15012 – Without Straps
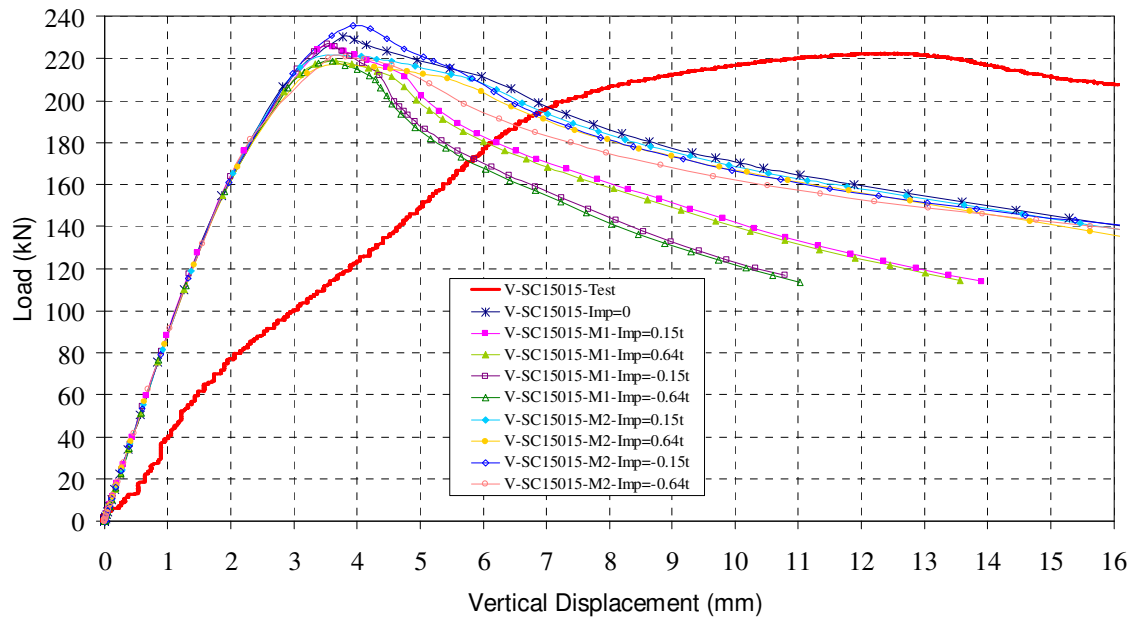
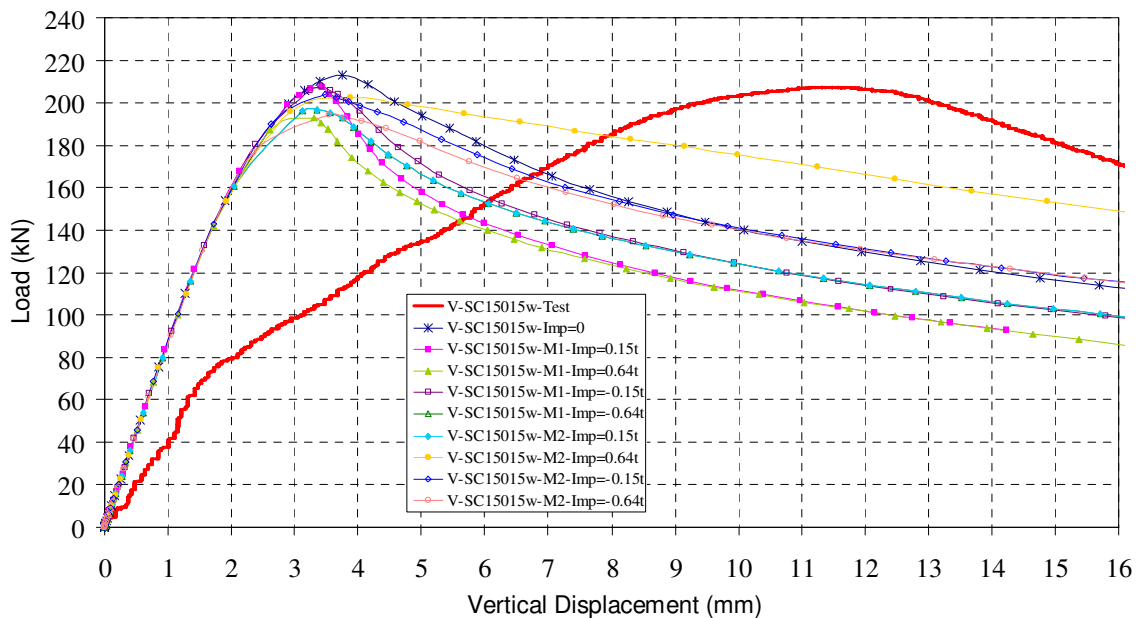Figure 31. Load and Vertical Displacement Relations of V-SC15015 – With Straps

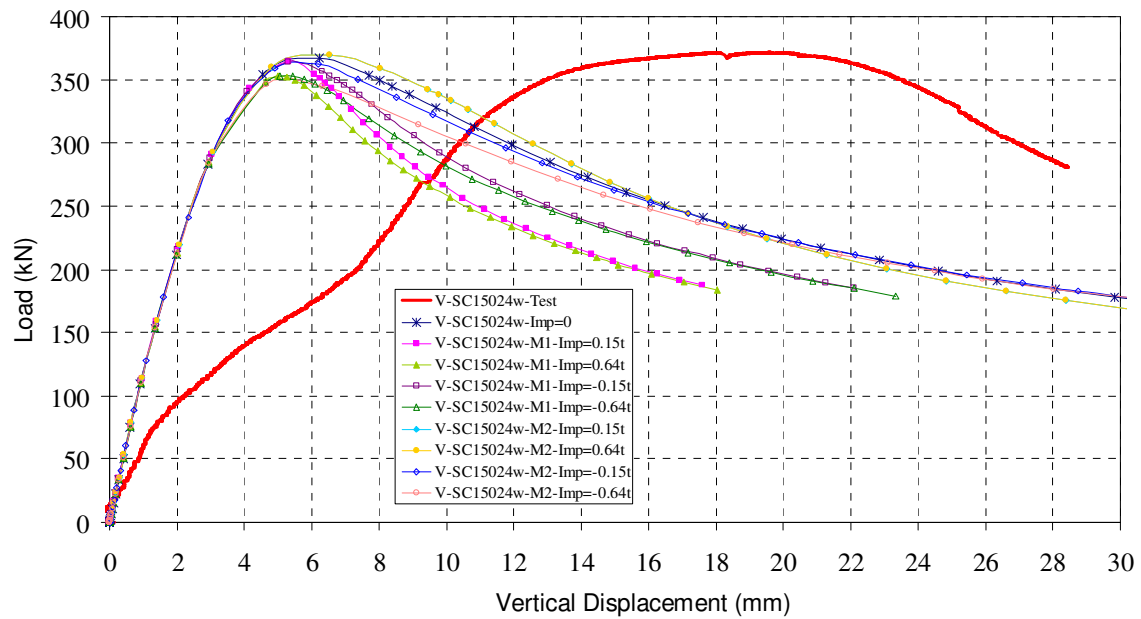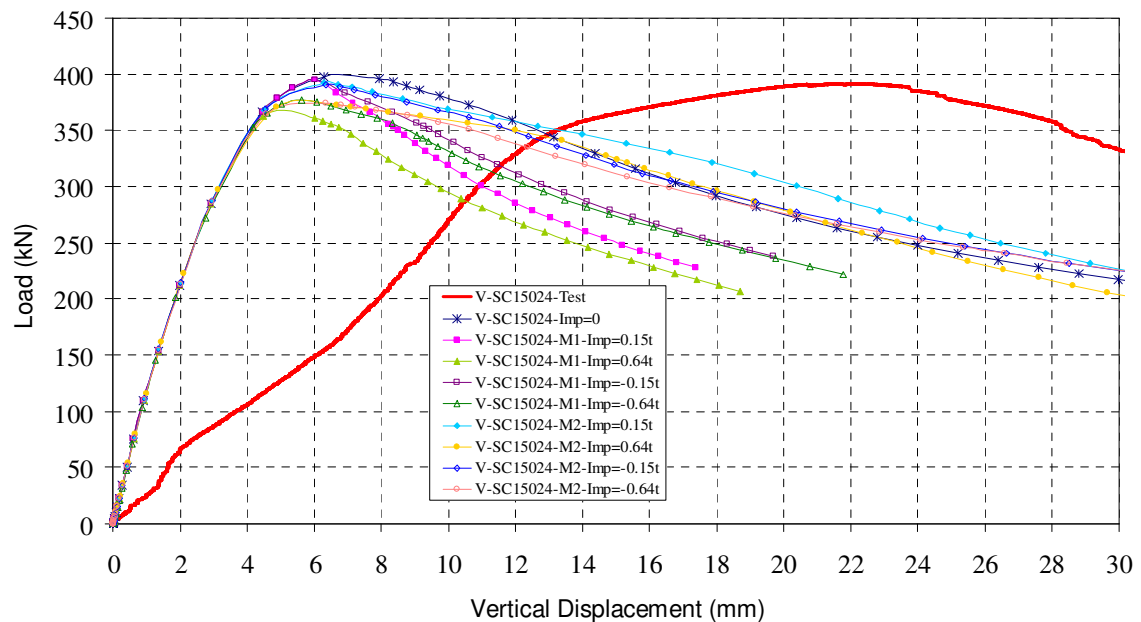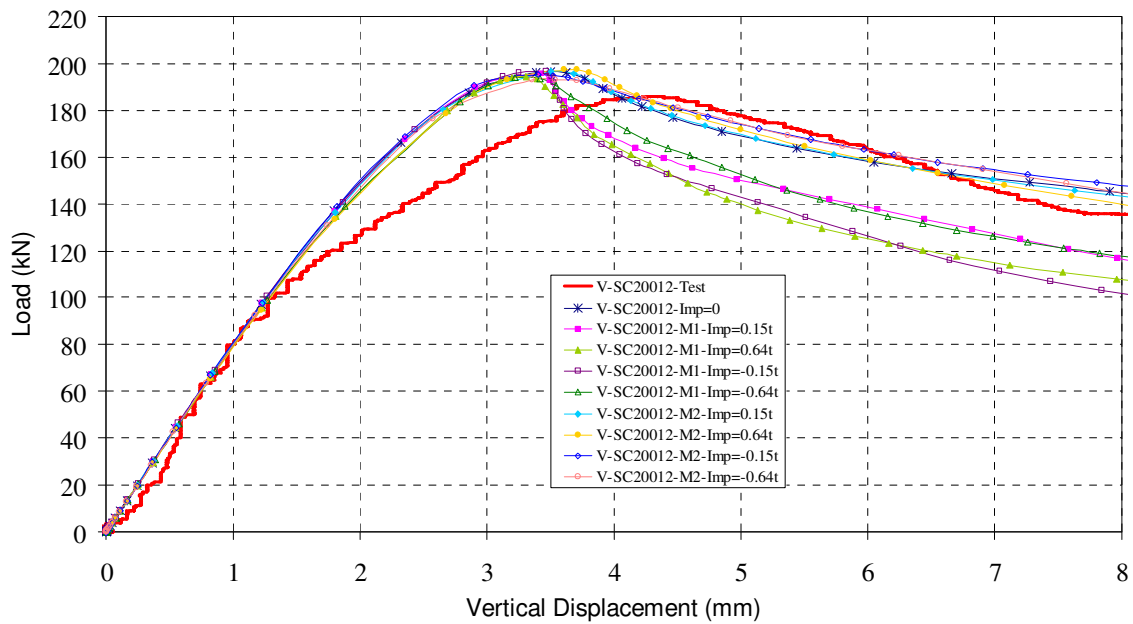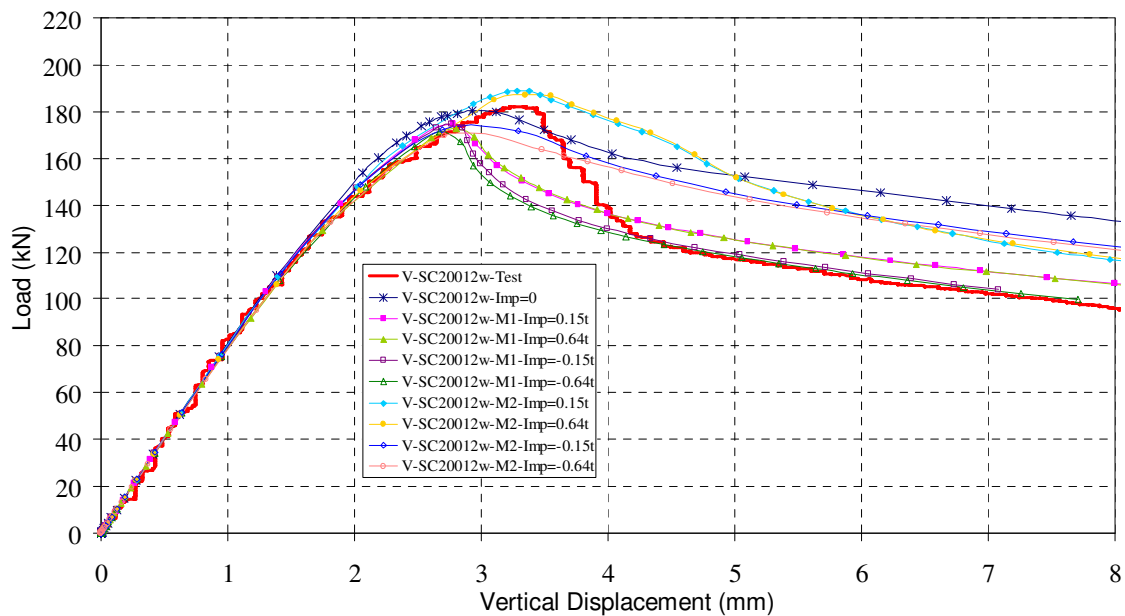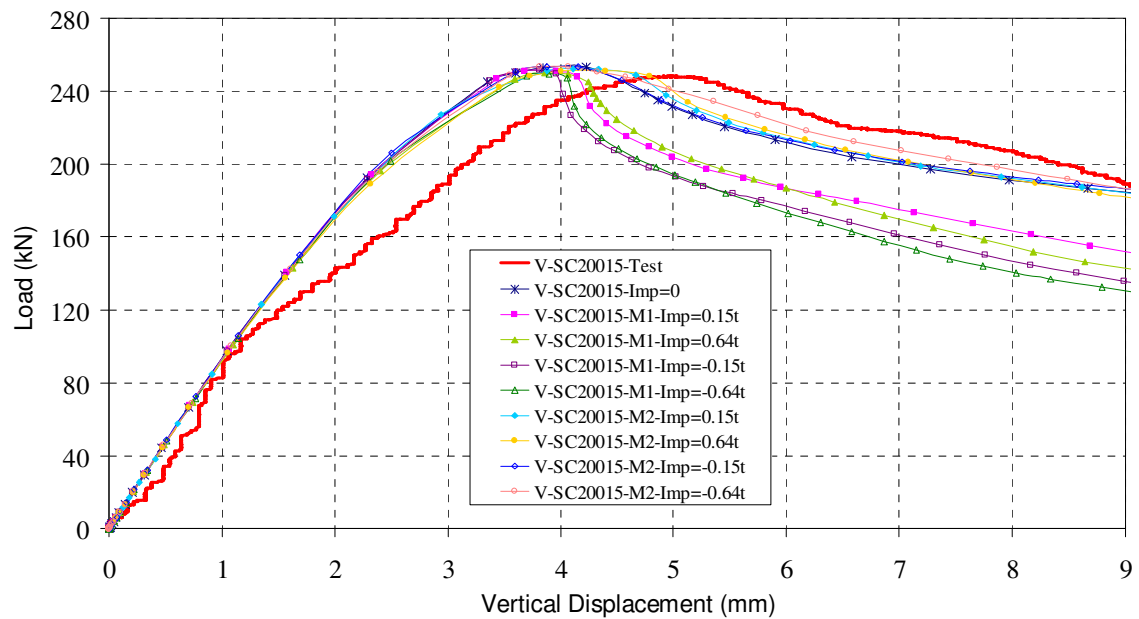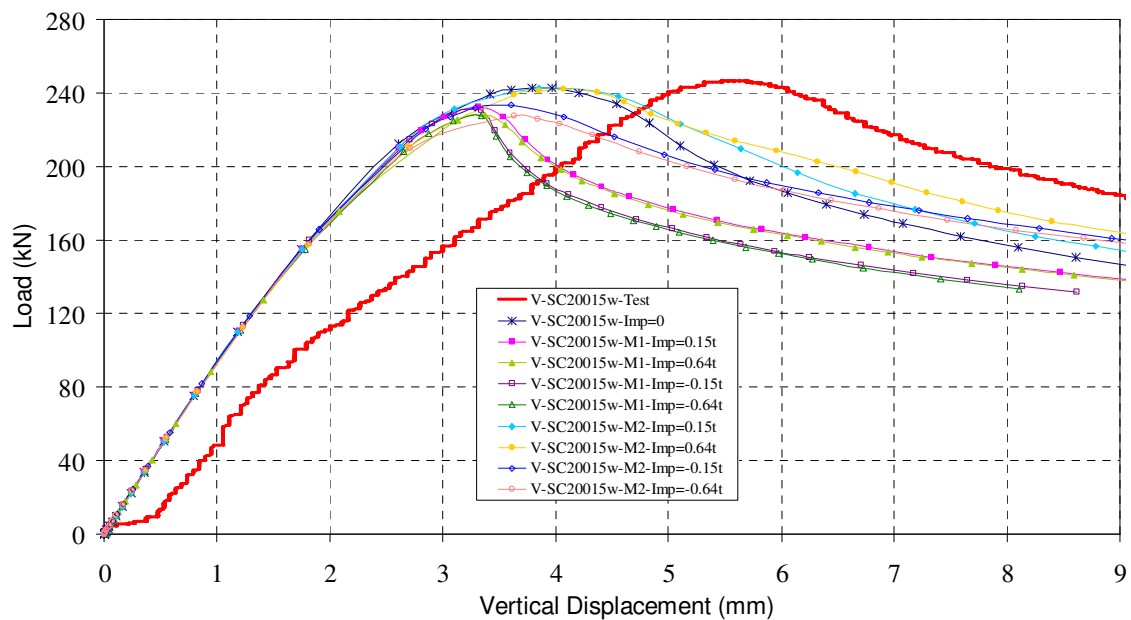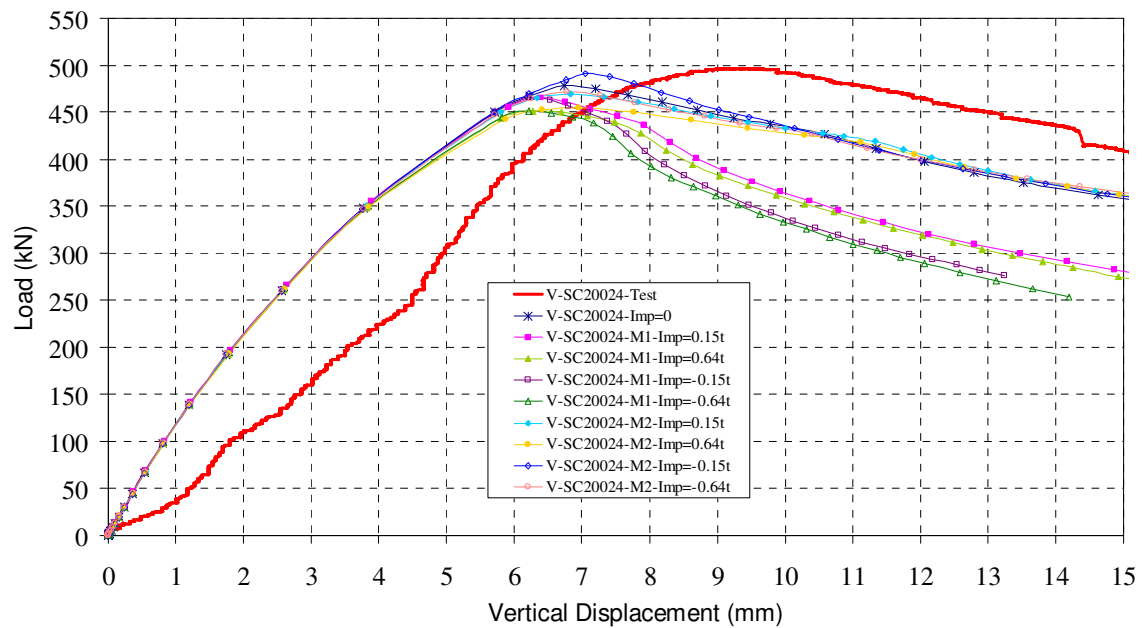Figure 32. Load and Vertical Displacement Relations of V-SC15015 – Without Straps

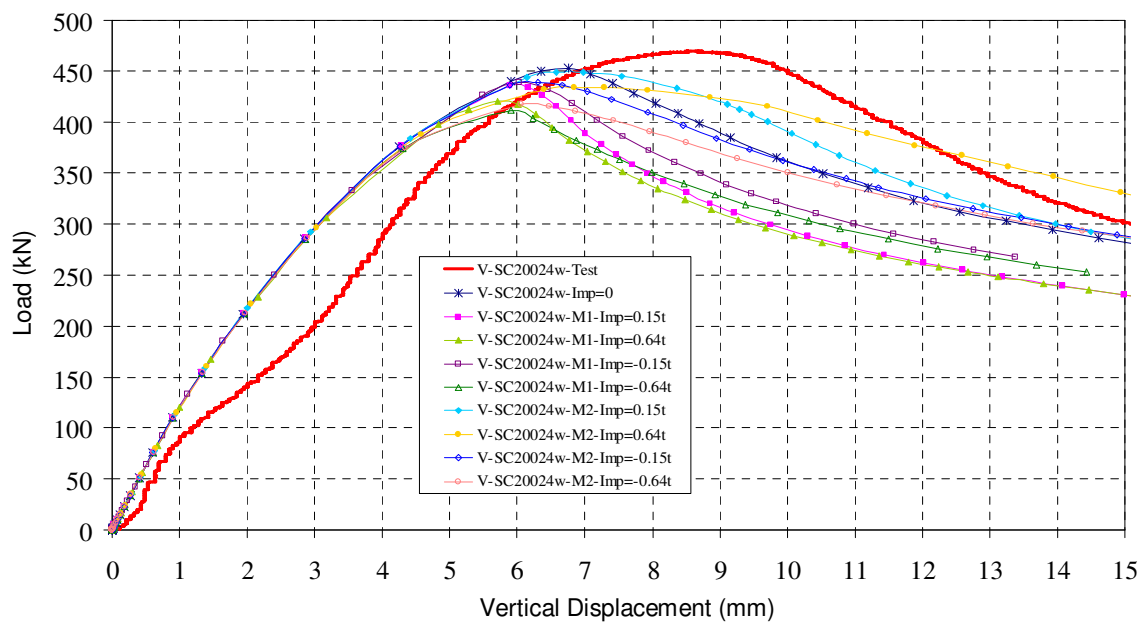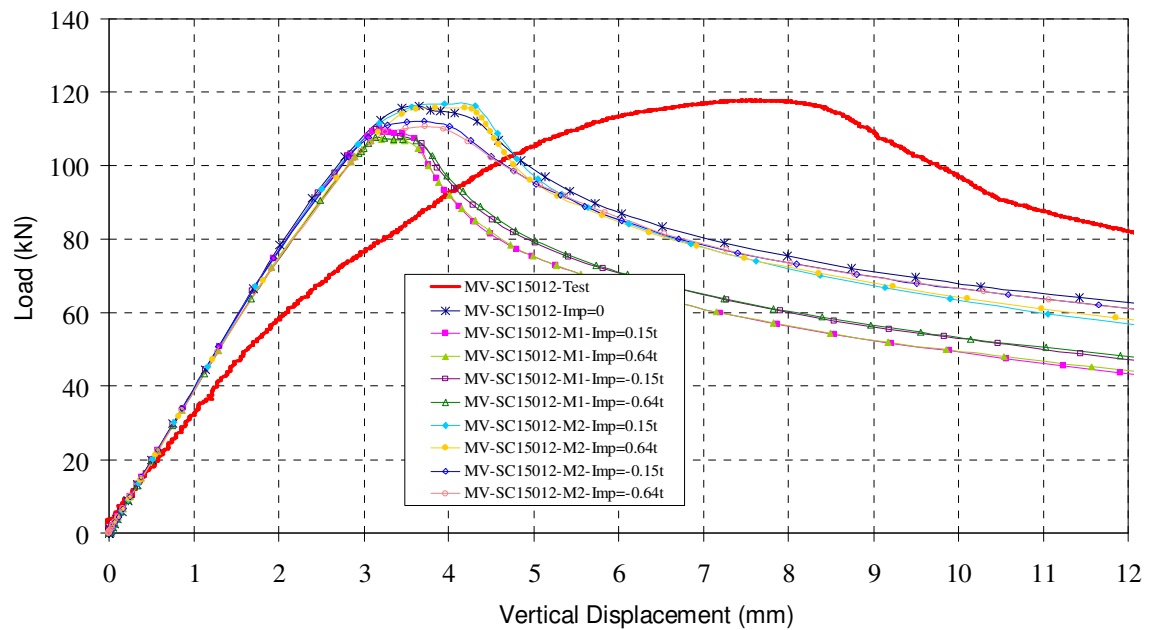Figure 33. Load and Vertical Displacement Relations of V-SC15024 – With Straps

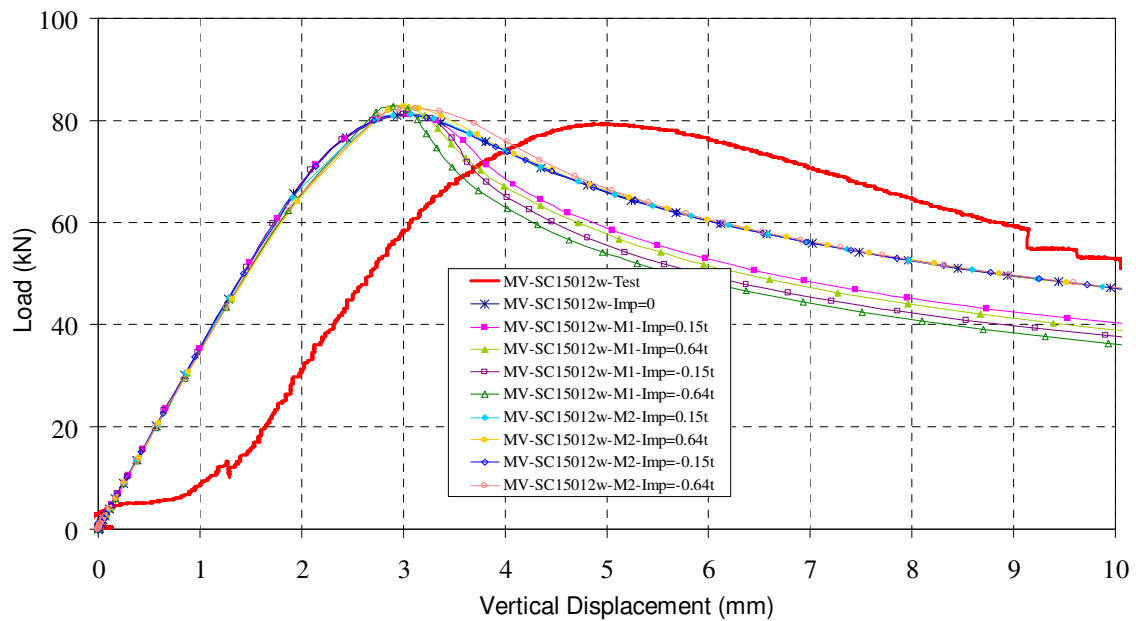
Figure 34. Load and Vertical Displacement Relations of V-SC15024 – Without Straps
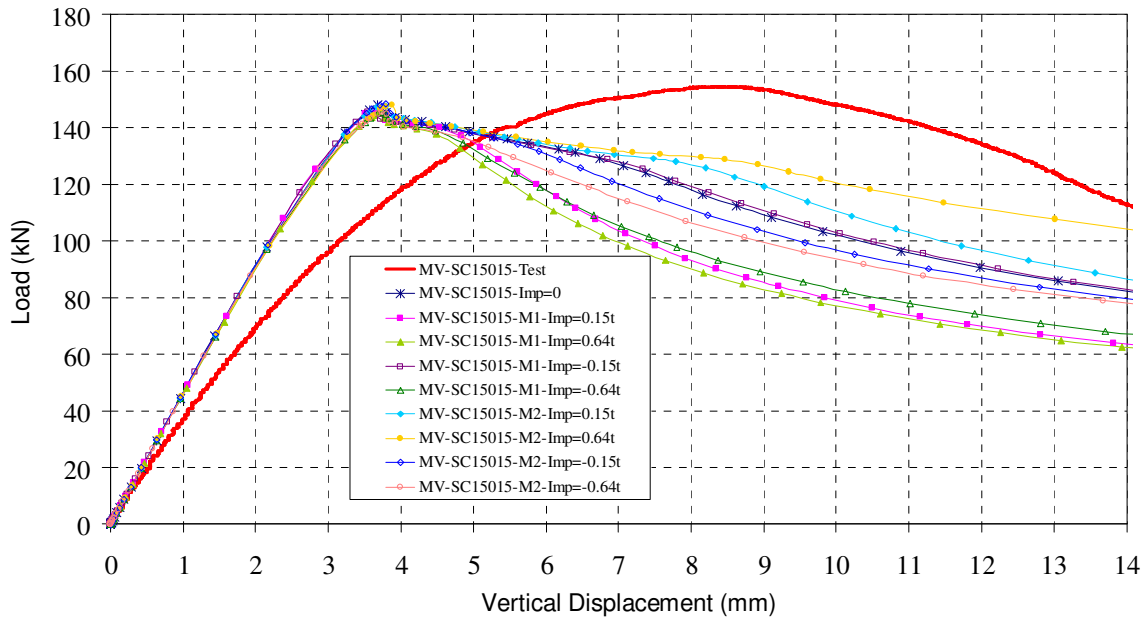
Figure 35. Load and Vertical Displacement Relations of V-SC20012 – With Straps

Figure 36. Load and Vertical Displacement Relations of V-SC20012 – Without Straps

Figure 37. Load and Vertical Displacement Relations of V-SC20015 – With Straps

Figure 38. Load and Vertical Displacement Relations of V-SC20015 – Without Straps

Figure 39. Load and Vertical Displacement Relations of V-SC20024 – With Straps

Figure 40. Load and Vertical Displacement Relations of V-SC20024 – Without Straps

Figure 41. Load and Vertical Displacement Relations of MV-SC15012 – With Straps

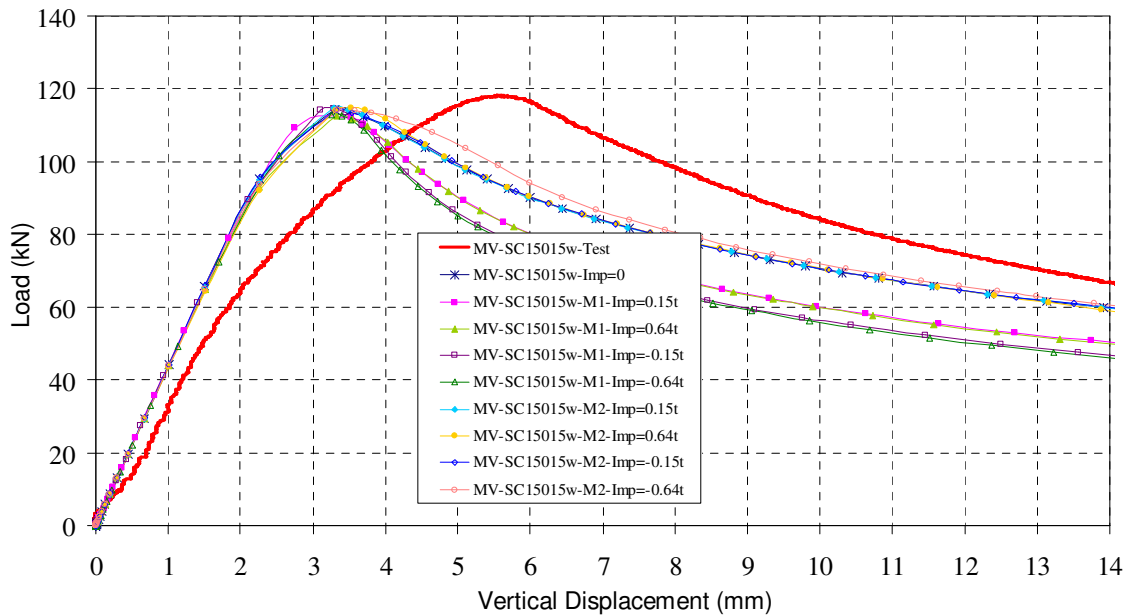

Figure 42. Load and Vertical Displacement Relations of MV-SC15012 – Without Straps

Figure 43. Load and Vertical Displacement Relations of MV-SC215015 – With Straps

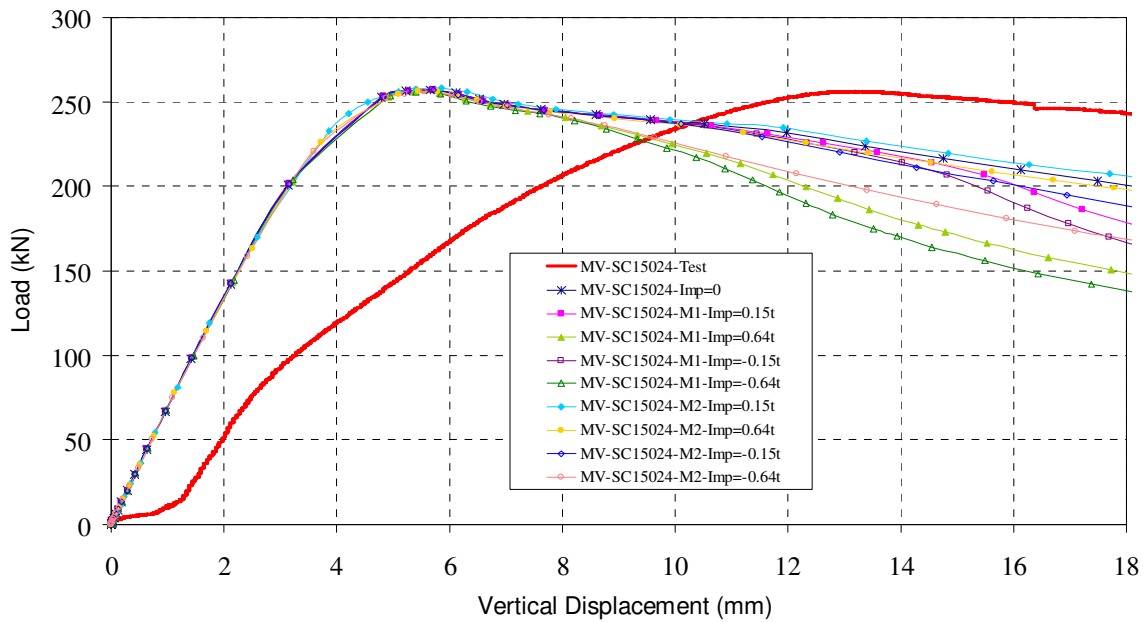Figure 44. Load and Vertical Displacement Relations of MV-SC15015 – Without Straps

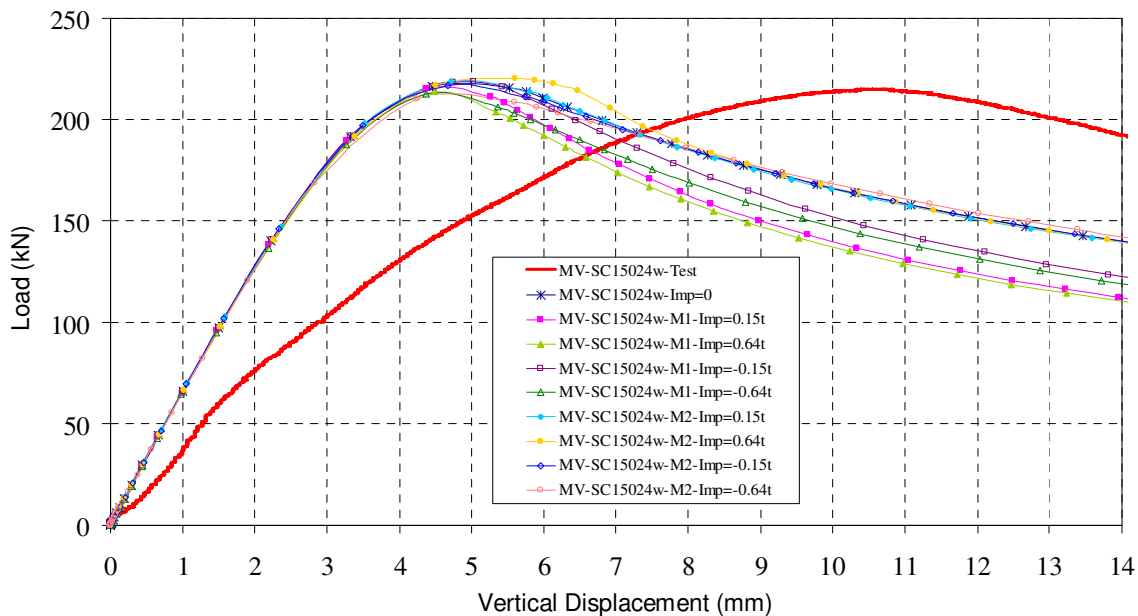Figure 45. Load and Vertical Displacement Relations of MV-SC15024 – With Straps

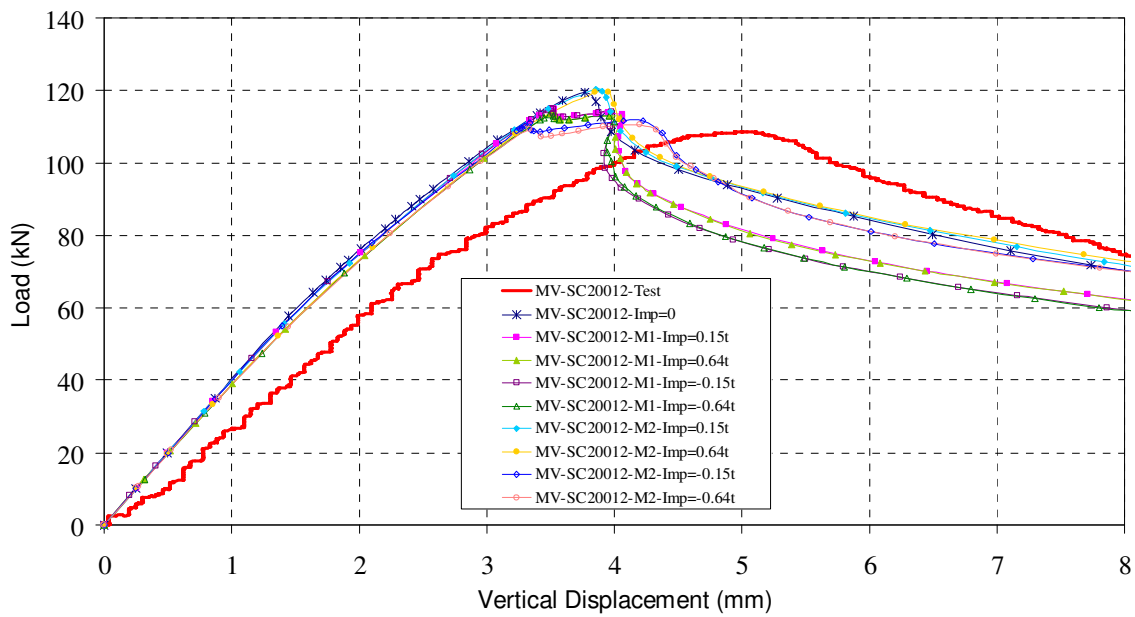Figure 46. Load and Vertical Displacement Relations of MV-SC15024 – Without Straps

Figure 47. Load and Vertical Displacement Relations of MV-SC20012 – With Straps
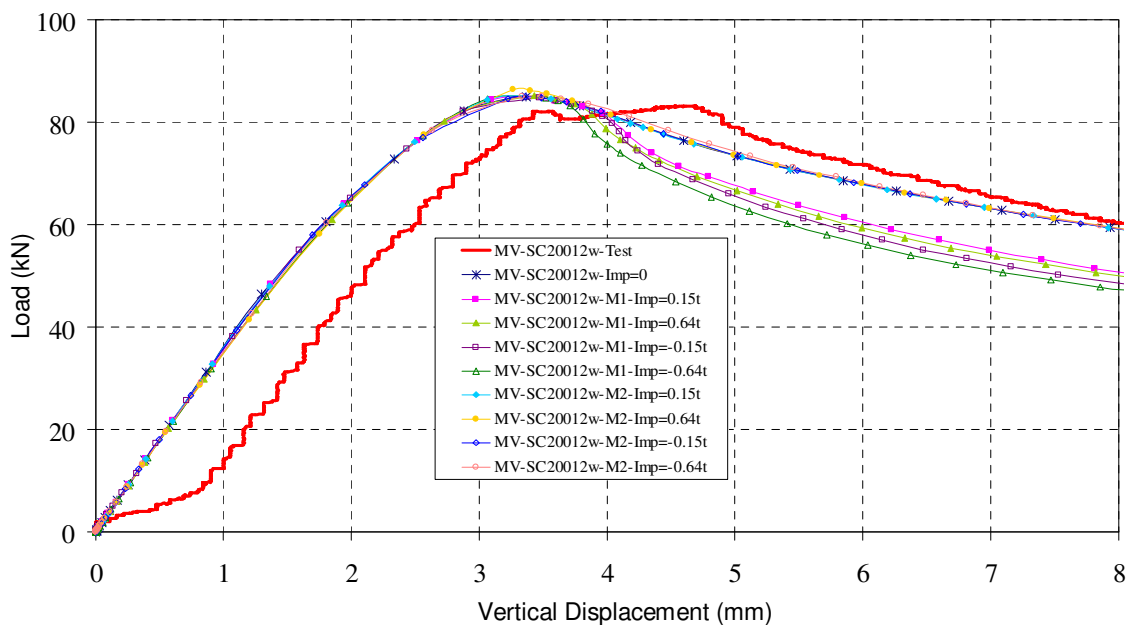

Figure 48. Load and Vertical Displacement Relations of MV-SC20012 – Without Straps
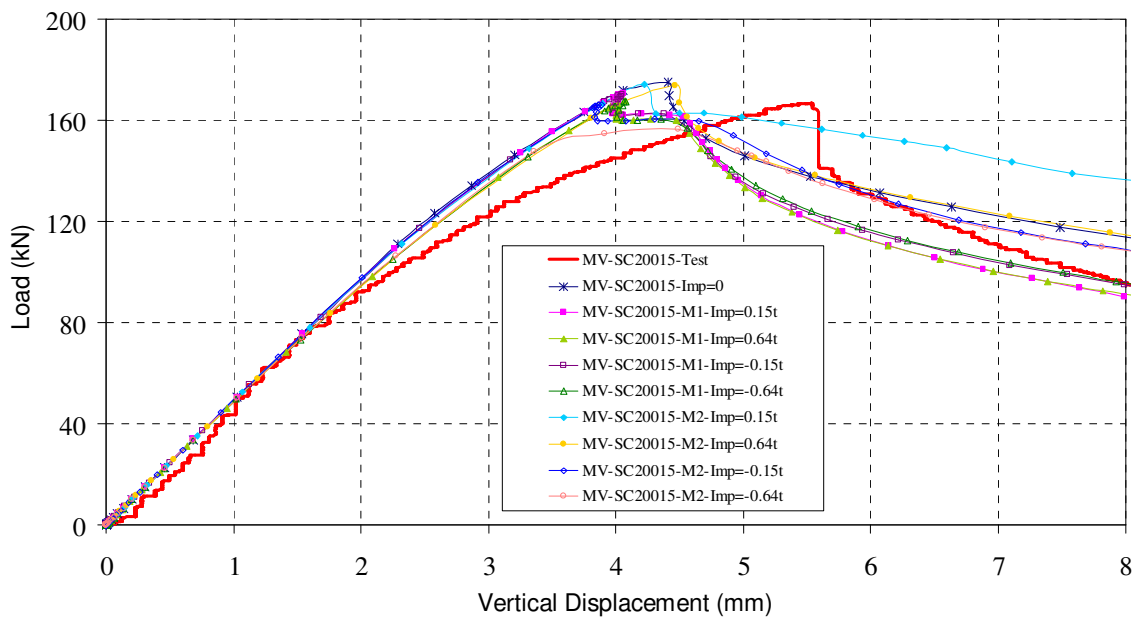
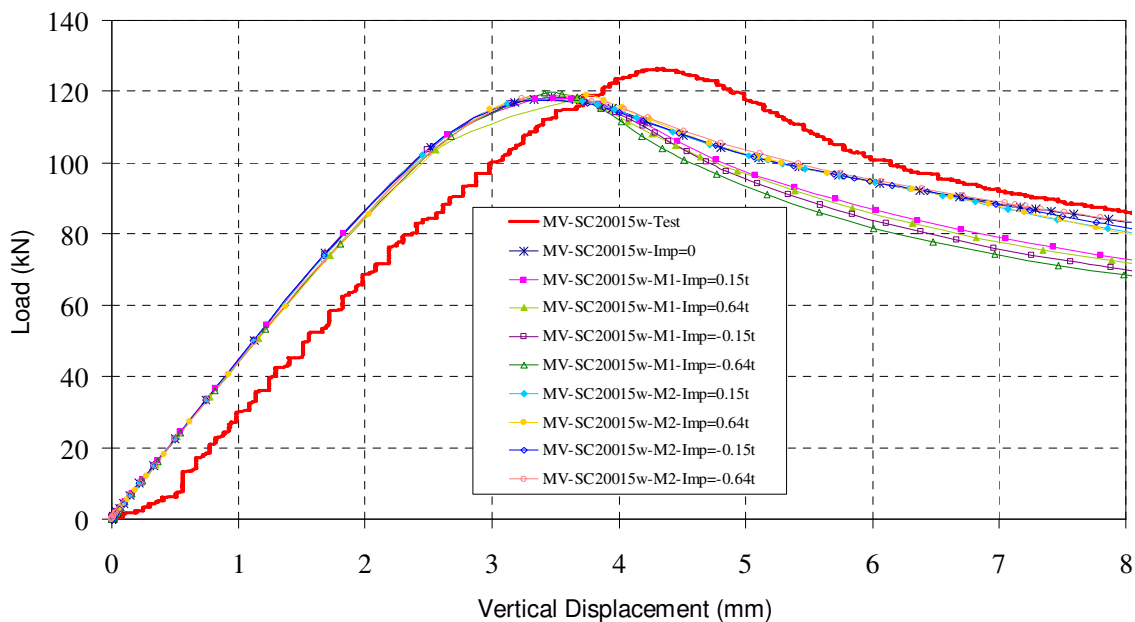Figure 49. Load and Vertical Displacement Relations of MV-SC20015 – With Straps

Figure 50. Load and Vertical Displacement Relations of MV-SC20015 – Without Straps
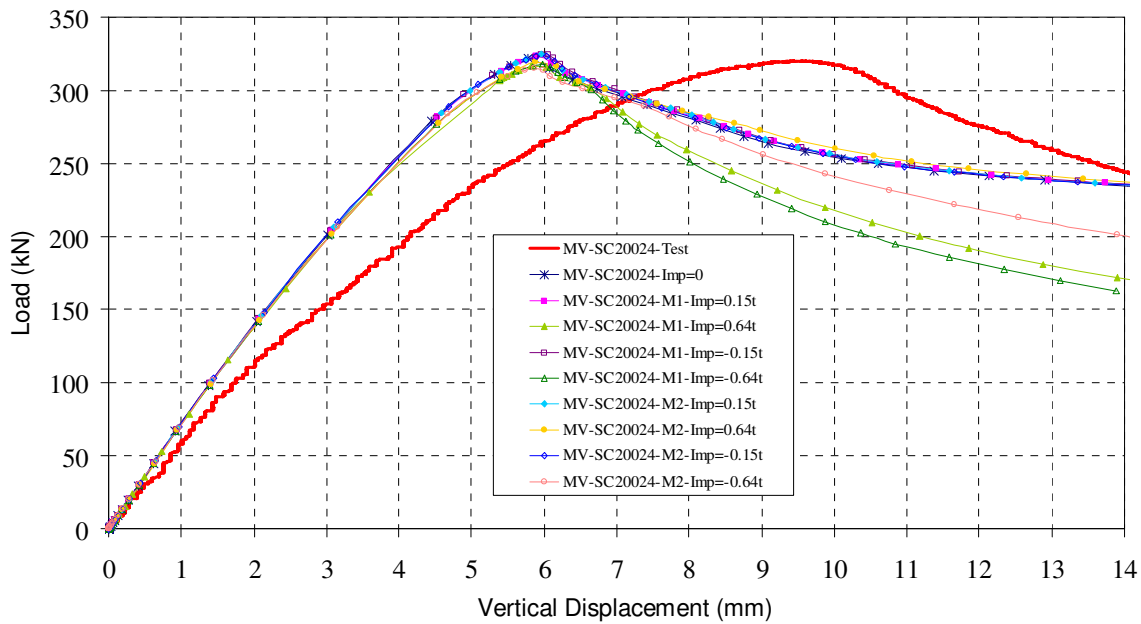
Figure 51. Load and Vertical Displacement Relations of MV-SC20024 – With Straps

Figure 52. Load and Vertical Displacement Relations of MV-SC20024 – Without Straps

Figure 53. Load and Vertical Displacement Relations of M-SC15012 – With Straps

Figure 54. Load and Vertical Displacement Relations of M-SC15012 – Without Straps

Figure 55. Load and Vertical Displacement Relations of M-SC15015 – With Straps

Figure 56. Load and Vertical Displacement Relations of M-SC15015 – Without Straps

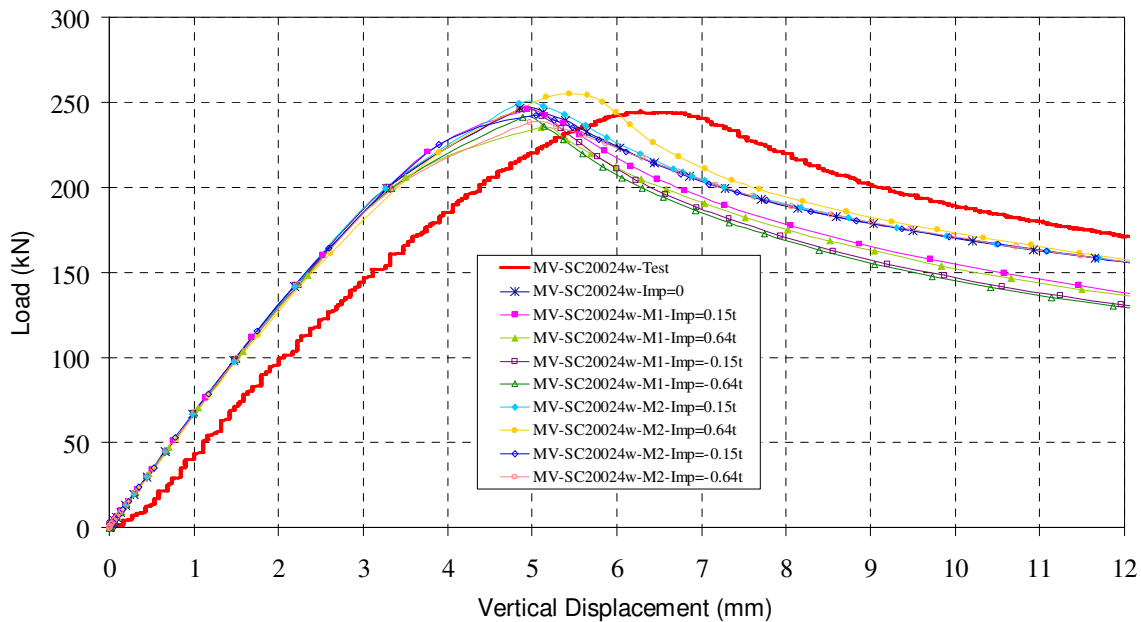Figure 57. Load and Vertical Displacement Relations of M-SC15024 – With Straps

Figure 58. Load and Vertical Displacement Relations of M-SC15024 – Without Straps

Figure 59. Load and Vertical Displacement Relations of M-SC20012 – With Straps

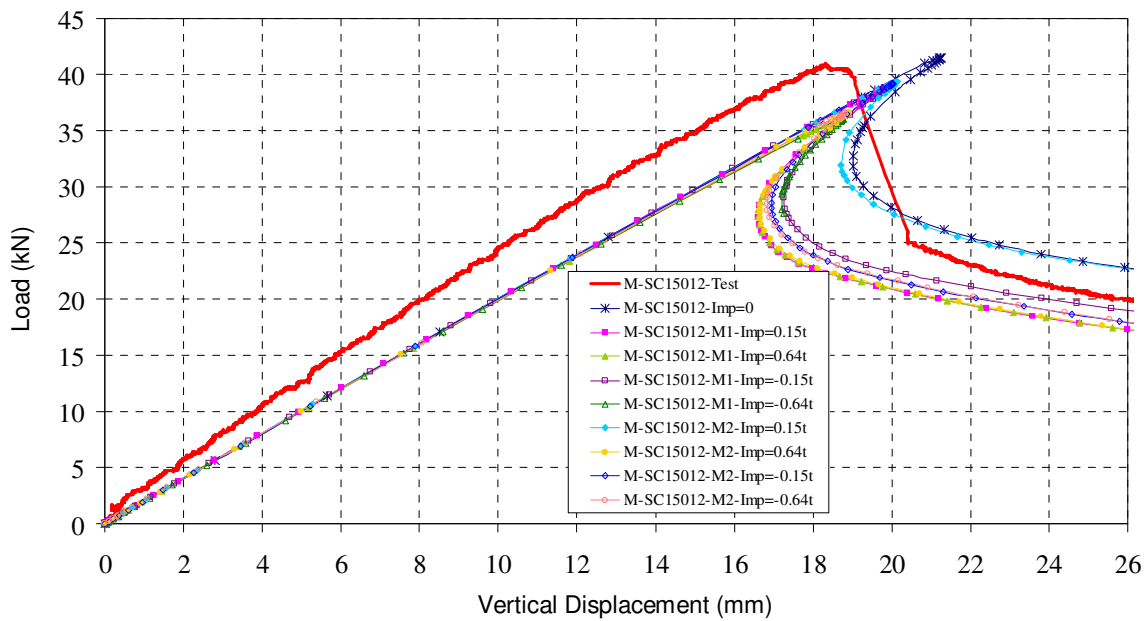Figure 60. Load and Vertical Displacement Relations of M-SC20012 – Without Straps

Figure 61. Load and Vertical Displacement Relations of M-SC20015 – With Straps

Figure 62. Load and Vertical Displacement Relations of M-SC20015 – Without Straps

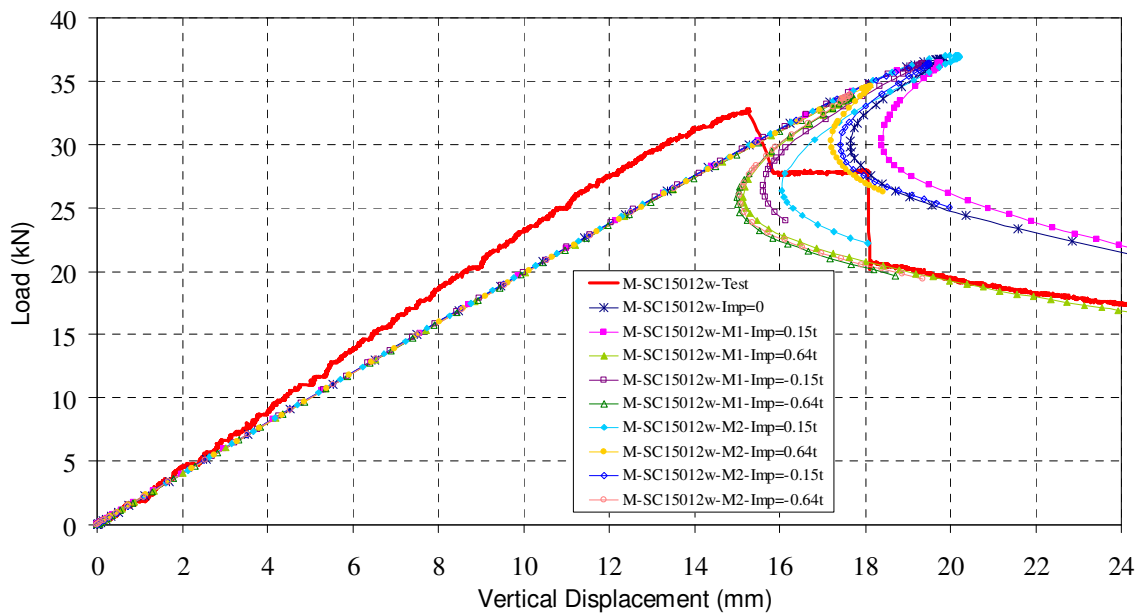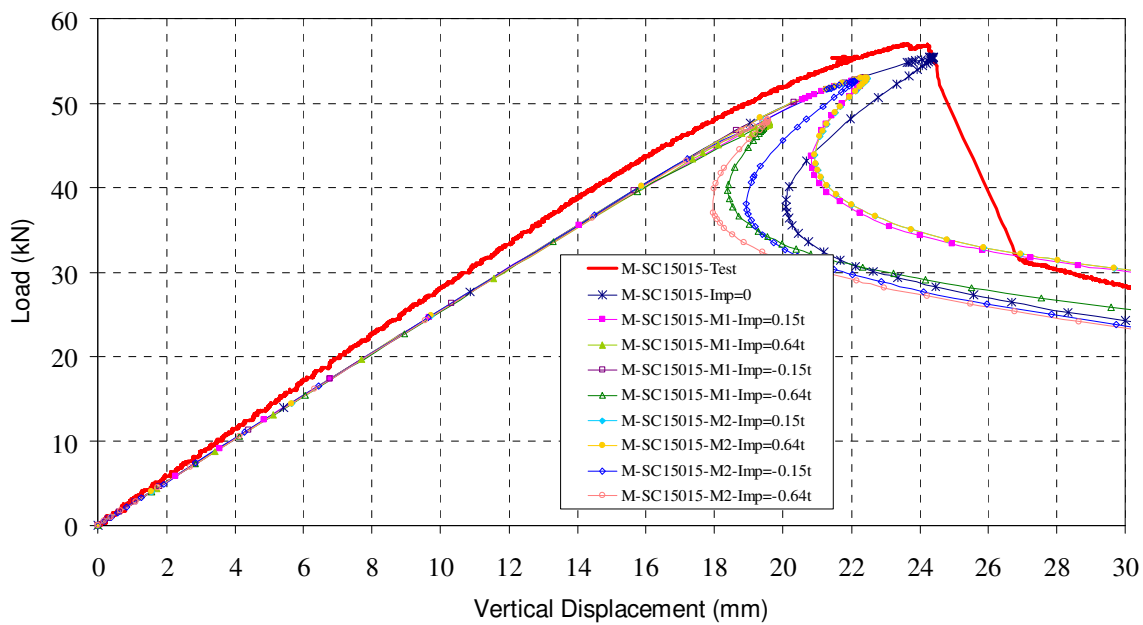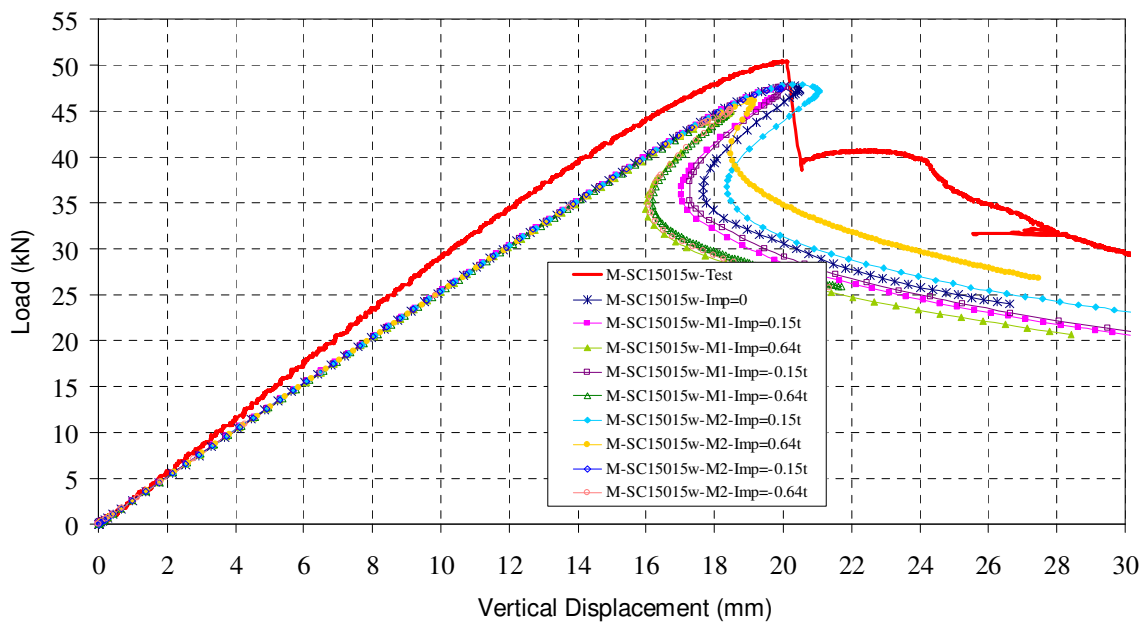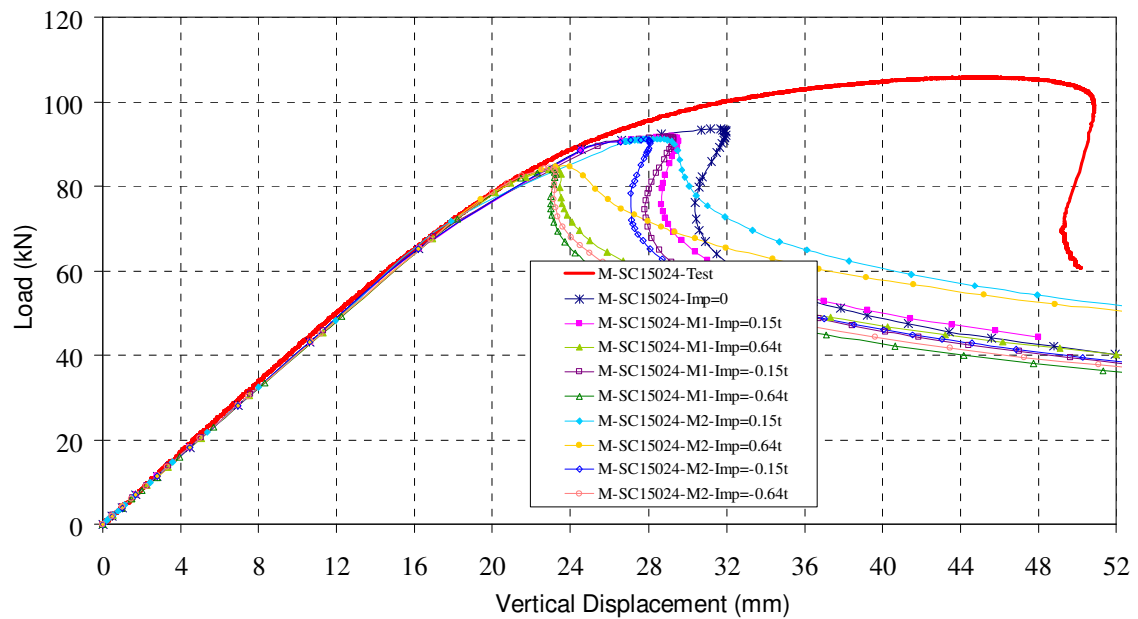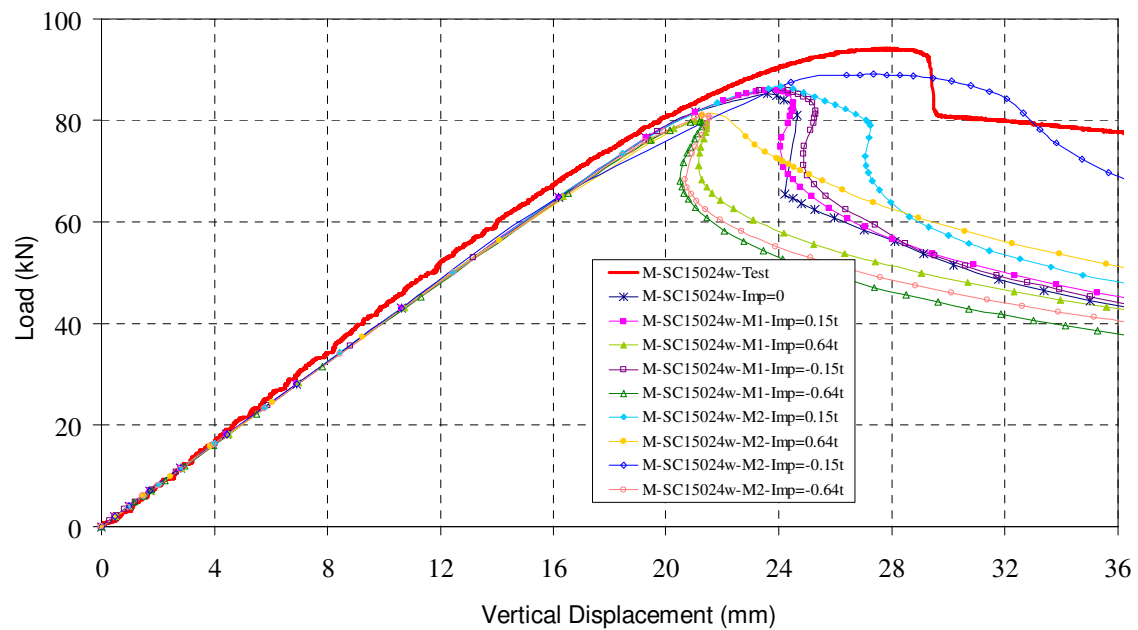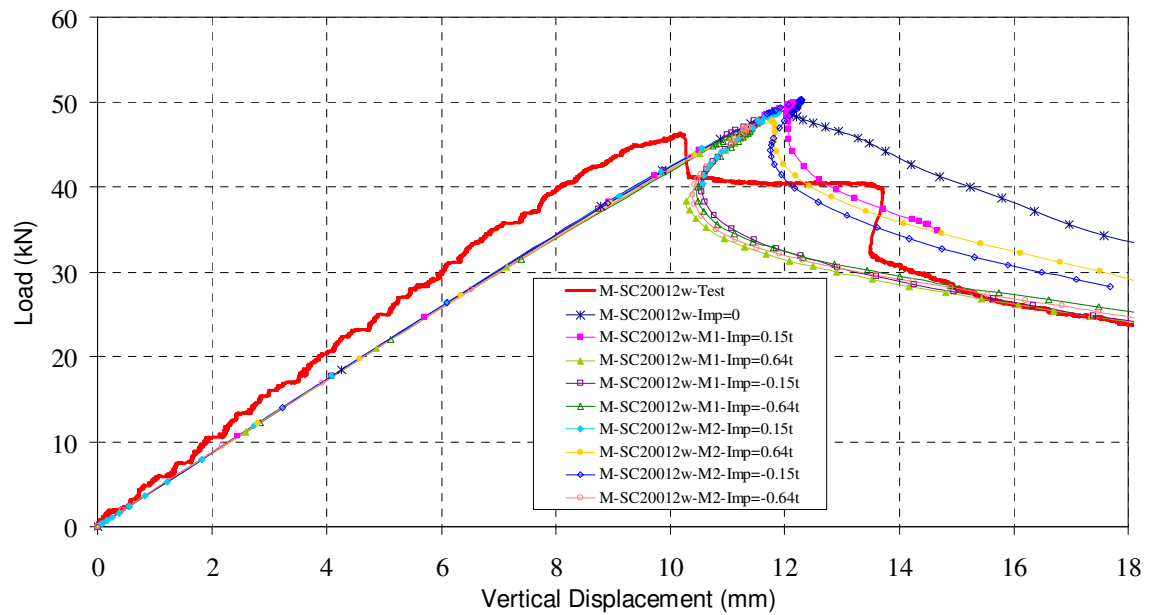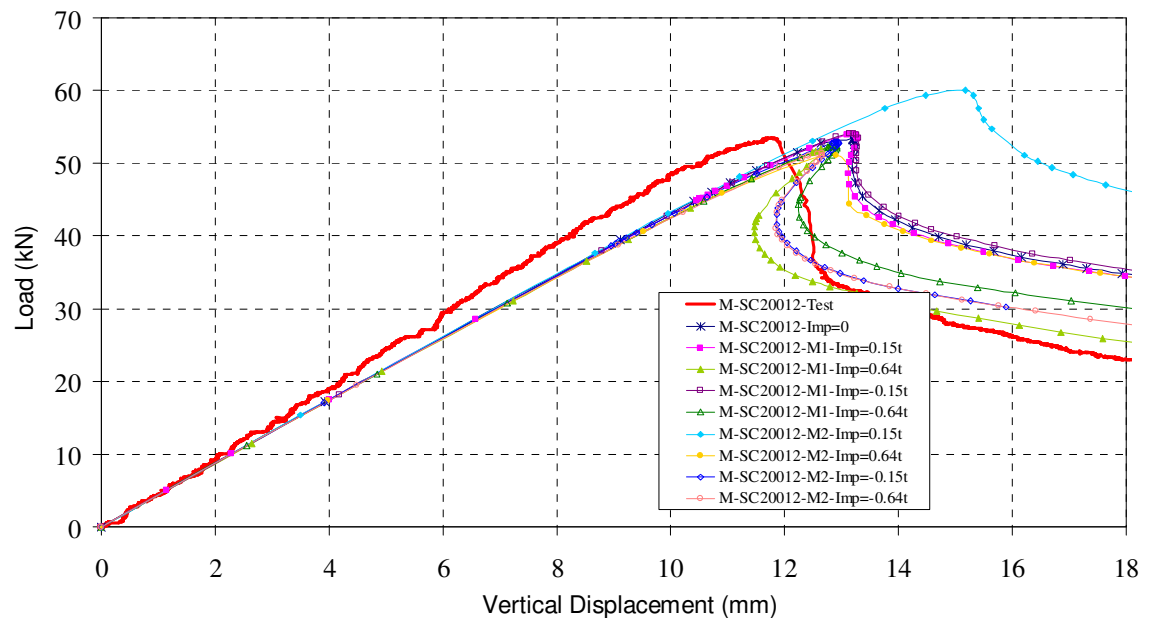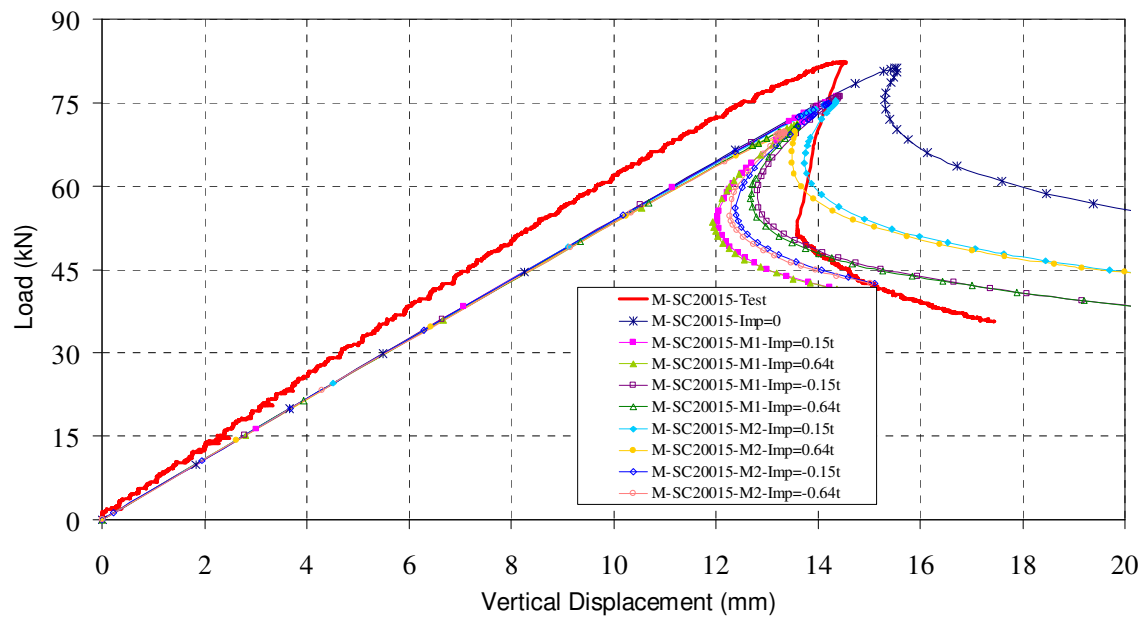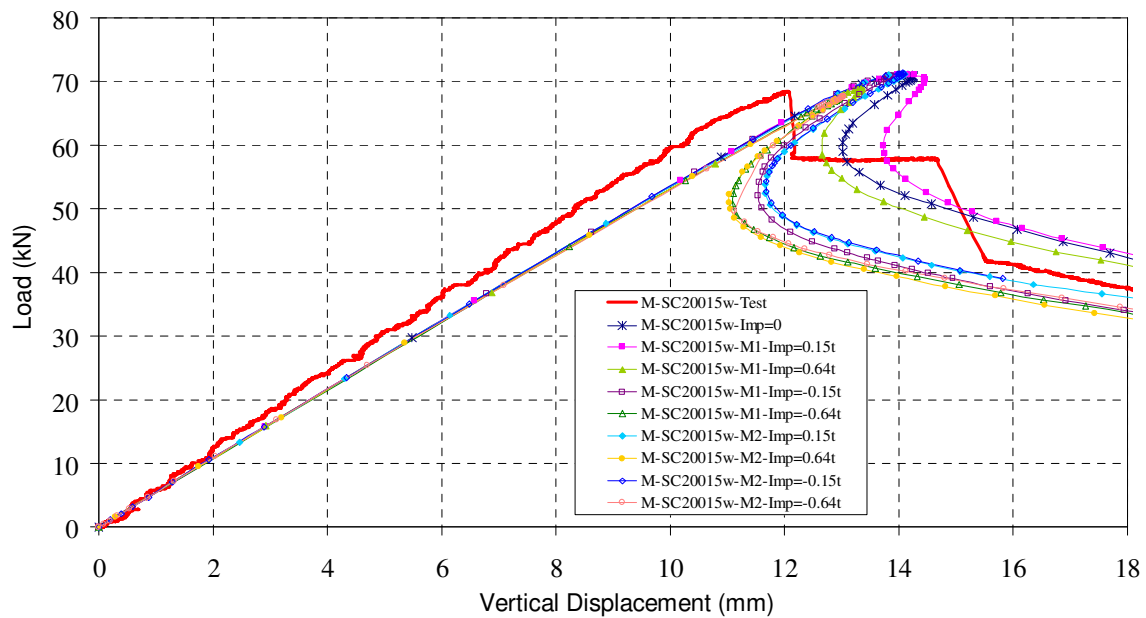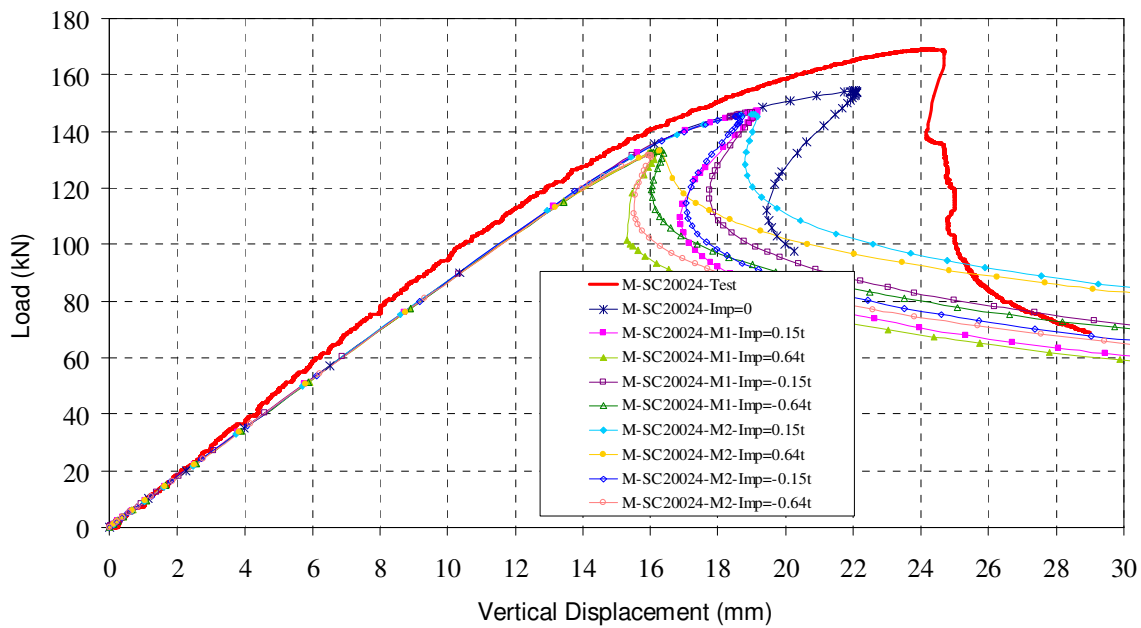Figure 63. Load and Vertical Displacement Relations of M-SC20024 – With Straps
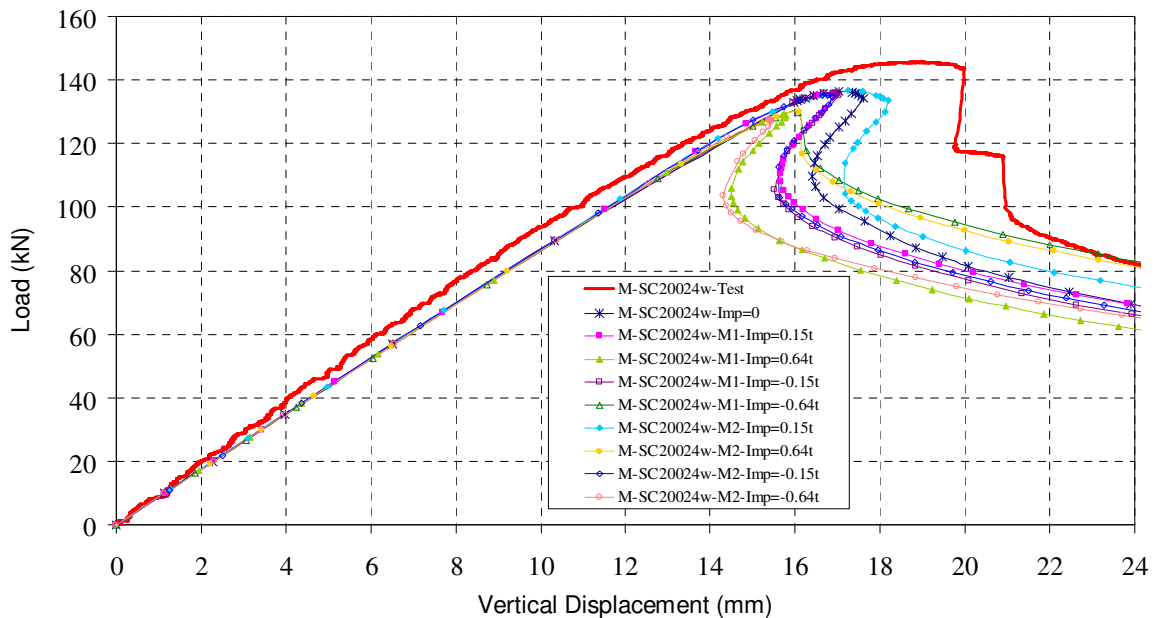
Figure 64. Load and Vertical Displacement Relations of M-SC20024 – Without Straps

APPENDIX 2: *V*TESTS AND FEM MAXIMUM LOADS

Section	Tests		FE Modeling								
	Test 1	Test w	Imp=0	Mode 1 Imp=0.15t	Mode 1 Imp=0.64t	Mode 1 Imp=-0.15t	Mode 1 Imp=-0.64t	Mode 2 Imp=0.15t	Mode 2 Imp=0.64t	Mode 2 Imp=-0.15t	Mode 2 Imp=-0.64t
	(kN)	(kN)	(kN)	(kN)	(kN)	(kN)	(kN)	(kN)	(kN)	(kN)	(kN)
V-SC15012	168.539	-	185.659	183.186	179.693	183.354	179.632	182.202	178.739	188.944	179.155
V-SC15012w	-	157.307	169.509	163.296	157.262	162.483	148.285	167.258	164.186	163.650	155.472
V-SC15015	222.317	-	230.091	225.614	218.531	226.888	218.438	220.962	215.523	235.859	220.613
V-SC15015w	-	207.484	213.136	207.302	193.058	207.592	196.843	196.843	202.680	204.112	194.146
V-SC15024	391.955	-	398.291	394.949	363.206	394.878	376.950	392.182	372.486	390.429	374.134
V-SC15024w	-	371.688	367.240	364.883	352.547	364.323	352.603	369.608	369.608	362.627	346.630
V-SC20012	185.936	-	196.581	195.638	194.555	196.729	194.030	196.395	197.481	195.226	193.321
V-SC20012w	-	182.212	180.156	174.916	172.582	174.999	171.184	189.063	187.344	172.350	169.682
V-SC20015	248.260	-	253.360	251.014	250.112	251.564	249.268	252.378	251.438	253.660	253.242
V-SC20015w	-	246.612	242.598	232.520	227.922	230.800	227.552	242.624	242.154	233.332	227.198
V-SC20024	496.826	-	478.328	465.410	451.084	465.132	451.056	469.662	454.734	490.686	471.776
V-SC20024w	-	469.235	452.598	436.180	420.134	439.040	411.054	448.896	434.188	439.162	416.862

APPENDIX 3: *MV* TESTS AND FEM MAXIMUM LOADS

Section	Tests		FE Modeling								
	Test 1	Test w	Imp=0	Mode 1 Imp=0.15t	Mode 1 Imp=0.64t	Mode 1 Imp=-0.15t	Mode 1 Imp=-0.64t	Mode 2 Imp=0.15t	Mode 2 Imp=0.64t	Mode 2 Imp=0.15t	Mode 2 Imp=-0.64t
	(kN)	(kN)	(kN)	(kN)	(kN)	(kN)	(kN)	(kN)	(kN)	(kN)	(kN)
MV-SC15012	117.873	-	116.247	110.305	107.008	109.775	107.759	116.720	115.808	112.115	110.633
MV-SC15012w	-	79.355	80.863	81.062	82.534	81.077	82.814	81.123	82.730	80.521	82.405
MV-SC15015	154.499	-	148.093	145.011	145.182	145.290	145.515	147.598	148.057	148.297	145.451
MV-SC15015w	-	118.178	114.369	111.976	112.686	114.562	112.947	114.664	114.813	114.115	114.134
MV-SC15024	256.196	-	257.350	256.979	255.701	257.088	255.630	258.245	256.397	256.890	256.022
MV-SC15024w	-	214.809	216.163	215.264	213.837	218.568	212.757	218.558	220.080	216.986	210.179
MV-SC20012	108.595	-	119.515	114.998	113.624	114.947	113.345	120.312	119.572	111.798	110.651
MV-SC20012w	-	83.262	85.081	84.306	85.225	84.702	84.797	84.523	86.497	84.970	84.991
MV-SC20015	166.707	-	175.138	170.471	167.709	170.261	167.356	174.164	173.668	166.182	156.484
MV-SC20015w	-	126.480	118.261	118.238	117.697	116.811	119.552	117.321	119.071	116.596	118.145
MV-SC20024	320.107	-	322.374	323.264	316.310	324.146	317.940	324.894	319.204	323.750	315.184
MV-SC20024w	-	244.781	246.246	245.568	235.328	245.674	240.900	249.112	254.880	242.336	238.388

APPENDIX 4: *M* TESTS AND FEM MAXIMUM LOADS

Section	Tests			FE Modeling								
	Test 1	Test w	Imp=0	Mode 1 Imp=0.15t	Mode 1 Imp=0.64t	Mode 1 Imp=-0.15t	Mode 1 Imp=-0.64t	Mode 2 Imp=0.15t	Mode 2 Imp=0.64t	Mode 2 Imp=-0.15t	Mode 2 Imp=-0.64t	
	(kN)	(kN)	(kN)	(kN)	(kN)	(kN)	(kN)	(kN)	(kN)	(kN)	(kN)	
M-SC15012	40.960	-	41.487	39.003	36.119	39.057	36.078	39.332	36.609	39.224	36.547	
M-SC15012w	-	32.780	36.768	36.477	33.871	36.379	33.898	37.007	34.588	36.441	33.920	
M-SC15015	57.014	-	55.447	52.930	47.705	52.965	47.368	53.024	53.024	52.666	47.998	
M-SC15015w	-	50.482	47.742	47.576	45.059	47.583	45.026	47.916	46.127	47.463	45.113	
M-SC15024	105.970	-	93.505	91.758	84.030	91.690	83.938	91.244	84.698	91.033	84.306	
M-SC15024w	-	94.189	85.327	85.919	79.914	86.187	79.848	86.588	81.015	89.010	80.753	
M-SC20012	53.534	-	53.381	53.896	52.391	54.011	52.402	60.071	51.103	52.969	51.315	
M-SC20012w	-	46.331	49.652	49.906	47.014	47.861	46.958	48.800	47.736	50.249	47.008	
M-SC20015	82.408	-	81.275	76.087	71.081	76.114	70.957	75.361	69.919	74.879	69.667	
M-SC20015w	-	68.490	70.968	71.070	69.022	70.818	67.471	71.243	67.626	71.246	67.673	
M-SC20024	169.088	-	154.180	147.039	133.355	146.815	133.368	146.102	132.901	145.493	131.472	
M-SC20024w	-	145.770	136.635	135.517	129.022	135.942	129.892	136.829	130.195	135.333	127.542	